frontiers | Frontiers in Materials

TYPE Review
PUBLISHED 26 August 2024
DOI 10.3389/fmats.2024.1444769

Check for updates

OPEN ACCESS

EDITED BY
Milan Radovic,
Paul Scherrer Institut (PSI), Switzerland

REVIEWED BY
Jacobo Santamaria,
Complutense University of Madrid, Spain
Shijing Gong,
East China Normal University, China

*CORRESPONDENCE
Zhiming Wang,
zhiming.wang@nimte.ac.cn

RECEIVED 06 June 2024
ACCEPTED 13 August 2024
PUBLISHED 26 August 2024

CITATION
Han Y, Lao B, Zheng X, Li S, Li R-W and Wang Z (2024) Transition metal oxides: a new frontier in spintronics driven by novel quantum states and efficient charge-spin interconversion. *Front. Mater.* 11:1444769. doi: 10.3389/fmats.2024.1444769

Transition metal oxides: a new frontier in spintronics driven by novel quantum states and efficient charge-spin interconversion

Yamin Han[1,2,3], Bin Lao[1,2], Xuan Zheng[1,2], Sheng Li[1,2], Run-Wei Li[1,2,3,4] and Zhiming Wang[1,2,3]*

[1]CAS Key Laboratory of Magnetic Materials and Devices, Ningbo Institute of Materials Technology and Engineering, Chinese Academy of Sciences, Ningbo, China, [2]Zhejiang Province Key Laboratory of Magnetic Materials and Application Technology, Ningbo Institute of Materials Technology and Engineering, Chinese Academy of Sciences, Ningbo, China, [3]Center of Materials Science and Optoelectronics Engineering, University of Chinese Academy of Sciences, Beijing, China, [4]School of Future Technology, University of Chinese Academy of Sciences, Beijing, China

Transition metal oxides (TMOs) have emerged as promising candidates for spintronic applications due to their unique electronic properties and novel quantum states. The intricate interplay between strong spin-orbit coupling and electronic correlations in TMOs gives rise to distinct spin and orbital textures, leading to enhanced spin-momentum locking and efficient charge-spin interconversion. Remarkably, recent researches have unveiled the significant and highly tunable nature of charge-spin interconversion efficiency in TMOs, which can be manipulated through strategies such as electric field gating, epitaxial strain, and heterostructure engineering. This review provides a comprehensive overview of the recent advances in understanding the electronic band structures of TMOs and their correlation with charge-spin interconversion mechanisms. We summarize the tunability of these properties through various experimental approaches and discuss the potential implications for spintronic device applications. The insights gained from this review can guide future research efforts towards the development of high-performance, energy-efficient spintronic devices based on TMOs.

KEYWORDS

transition metal oxides, electronic structure, charge-spin interconversion, heterostructure engineering, spintronic devices

1 Introduction

The rapid development of the information technologies, such as artificial intelligence, the Internet of Things, and big data, has led to an exponential growth in data generation and processing requirements. This unprecedented growth has created an urgent need for the development of novel materials and devices capable of efficient and reliable information storage and processing. While the current mainstream information storage (SRAM, DRAM, etc.) and processing (CPU, GPU, etc.) devices is based on transistor CMOS technology, which manipulates the charge properties of electrons, they face significant challenges in meeting the ever-increasing performance demands of the information technology era. In the past decades, CMOS devices have achieved remarkable improvements in performance, with transistor density doubling every 18 months, following Moore's Law. This has been accomplished by miniaturizing transistor feature sizes to increase the number of transistors per unit area. However, as transistor dimensions approach the nanometer scale, further miniaturization poses unprecedented challenges related to device performance and reliability. First, the quantum tunneling effect becomes prominent, leading to a weakening of the channel's ability to control charge flow and an increase in leakage current; second, while increasing current density can enhance charge control, it also leads to a significant rise in Joule heating, which can compromise device durability and energy efficiency. To address these challenges and enable sustainable growth in device performance, various solutions have been proposed, spanning from fundamental scientific research to technological innovations (Agarwal et al., 2021). Among these, spintronics has emerged as a promising alternative to conventional charge-based electronics.

Spintronics exploits the spin property of electrons, alongside their charge, to achieve high-performance information storage and processing, has become a widely focused topic (Manipatruni et al., 2018; Dieny et al., 2020). A key focus in the field of spintronics is the efficient conversion between charge and spin current, which is essential for the generation, manipulation, and detection of spin-based information. The charge-spin interconversion is mediated by the spin-orbit coupling (SOC) effect, which couples the motion of electrons (charge) with their spin angular momentum. The efficiency and mechanisms of charge-spin interconversion are strongly dependent on the electronic band structure of materials with strong SOC and crucial for developing efficient spin-based devices.

In this context, transition metal oxides have garnered significant attention as promising candidates for spintronic applications. These materials exhibit a rich variety of physical properties arising from the complex interplay between charge, spin, orbital, and lattice degrees of freedom (Ramesh and Schlom, 2019). This coupling gives rise to diverse phenomena such as magnetism, ferroelectricity, superconductivity, and colossal magnetoresistance, which are closely related to electron correlation effects (Schilling et al., 1993; Tomioka et al., 1995; Li et al., 2004; Vrejoiu et al., 2006). Moreover, recent studies have revealed that the electronic structures of transition metal oxides can host various novel quantum states, such as topological insulators, Dirac and Weyl semimetals, and quantum anomalous Hall insulators, which are intimately connected to SOC and highly sensitive to external perturbations. These exotic electronic structures are expected to significantly influence the spin transport properties and charge-spin interconversion efficiency of transition metal oxides, offering new opportunities for the development of advanced spintronic devices (Chen and Yi, 2021; Trier et al., 2021).

In this review, we present a comprehensive overview of the recent progress in exploration of novel quantum states and charge-spin interconversion in transition metal oxides. We begin by introducing the fundamental concepts and mechanisms underlying the emergence of novel electronic states in these materials and their impact on spin-dependent transport properties. We then discuss the experimental and theoretical advances in understanding and harnessing charge-spin interconversion in representative transition metal oxide systems, focusing on perovskite oxides with 3*d*, 4*d*, and 5*d* transition metal ions. Finally, we highlight the challenges, opportunities, and the future directions in the development of transition metal oxide-based spintronic devices, emphasizing the importance of integrating theoretical insights with experimental techniques to unlock their full potential.

2 Mechanisms of electronic structure and charge-spin interconversion

2.1 Generation of novel electronic structures

In transition metal oxides, due to the intricate coupling between spin, orbital, charge, and lattice degrees of freedom gives rise to a plethora of quantum states that have not been anticipated in other material systems, such as Mott insulators, topological insulators, topological semimetals, and axion insulators (Witczak-Krempa et al., 2014). These unique electronic structures form the foundation for the emergence of novel physical properties and functionalities in transition metal oxides. Moreover, at the oxide heterojunction/surface, the breaking of spatial inversion symmetry introduces additional influences, leading to the formation of surface states differ from the bulk electronic structure. Among these electronic states, non-trivial topological band structures and Rashba surface states are of particular interest due to their ability to strongly influence the spin orientation and momentum of electrons. This spin-momentum locking effect endows the related oxide materials with the property of charge-spin interconversion, enabling the efficient manipulation of spin current through other means.

2.1.1 Non-trivial band structures

The generation of non-trivial band structures is usually based on the occurrence of band inversion, that is, the originally separated conduction and valence bands change their energy or width under the action of SOC, structural changes, and other factors, resulting in mutual crossing (Figure 1). When SOC is present in the system, it further opens up an energy gap at the crossing points. Depending on the extent of the gap opening, various topological states can emerge. If the energy gap is fully opened, topological insulators may be produced. If the energy gap is not fully opened, leaving some contact points, linear dispersion Dirac points or Weyl points will be produced. If some contact lines are left, Dirac nodal lines will be produced. The generation of Dirac and Weyl states has different symmetry requirements: Dirac points require the material to simultaneously satisfy spatial inversion symmetry and time-reversal symmetry, while Weyl points require the breaking of spatial inversion symmetry or time-reversal symmetry. In other words, a Dirac point can be transformed into two Weyl points by breaking the symmetries (Yan and Felser, 2017; Armitage et al., 2018). Thus, by tuning the SOC strength and symmetry, one can control the electronic structure and realize the generation and transformation of novel quantum states.

These topological band structures can produce large Berry curvature, which determines the intrinsic spin Hall effect (Xiao et al., 2010; Sinova et al., 2015). Therefore, when the Fermi surface is located near these topological band structures, it will

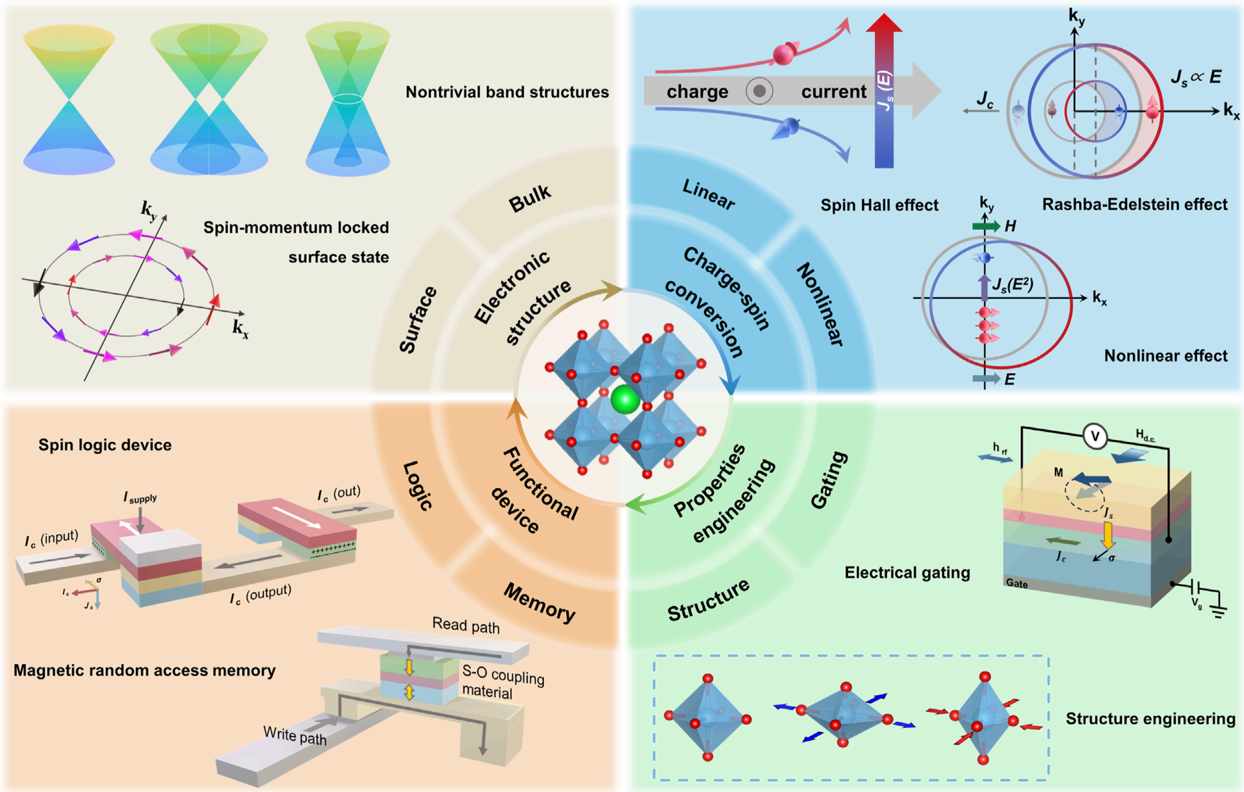

FIGURE 1
Transition metal oxides: Exploring novel electronic structures, charge-spin interconversion mechanisms, manipulation strategies, and their potential for advanced spintronic devices.

significantly affect the material's charge-spin interconversion properties. Although non-trivial band structures also exist in other material systems, the complex interplay of multiple degrees of freedom in transition metal oxides makes their electronic structure highly sensitive and tunable. Consequently, topological properties in these materials can be generated, changed, and enhanced through flexible regulation methods.

2.1.2 Surface states

Due to the inability of the non-trivial topological electronic structure to undergo continuous transformation at the vacuum or heterogeneous material interface, the naturally existing spatial inversion symmetry broken at the interface/surface will lead to surface states different from the bulk electronic structure. In topological materials with time-reversal symmetry, the energy $E(k,s) = E(-k,-s)$, where k represents momentum and s represents spin. The symmetry breaking at the interface will lead to $E(k,s) \neq E(-k,s)$, resulting in the lifting of spin degeneracy at a given momentum, a phenomenon known as spin splitting. Unlike the spin splitting in magnetic materials, the unbroken time-reversal symmetry requires the spin at each momentum to point in a specific orientation to satisfy the same spin occupancy on the Fermi surface, a phenomenon called spin-momentum locking. A similar situation occurs in Weyl semimetals with broken time-reversal symmetry, where the surface states are Fermi arcs connecting two Weyl points. As a result of this chirality difference, the electronic states along the Fermi arcs exhibit a gradual change in spin orientation, leading to a spin texture that is locked to the momentum direction. Moreover, in topologically trivial materials, based on the above inference about symmetry, spin-momentum locked surface states, i.e., Rashba surface states, also exist at the interface (Figure 1). The generation of such surface states can be described by a semi-classical model: at the symmetry-broken interface, due to the discontinuity of the chemical potential, a vertical electric field will be generated. When electrons move laterally at the interface, taking the electron as a localized reference system, the electric field produces an effective magnetic field perpendicular to the electron velocity, which can be approximately expressed as $B = -\frac{1}{c^2}v \times E$ at low velocities (Manchon et al., 2015). The interaction between this magnetic field and the electron spin will produce Zeeman splitting, with the spin splitting direction depending on the electron's momentum direction, resulting in spin-momentum locking.

2.2 Mechanisms of charge-spin interconversion

2.2.1 Spin Hall effect

When a charge current passes through a material with strong SOC, electrons with different spin orientations will deflect in opposite directions, producing a spin current. This phenomenon is called the spin Hall effect (Figure 1). In the spin Hall effect, the charge current direction, spin current direction, and spin direction satisfy a mutually perpendicular relationship. The generated spin current enters the neighboring magnetic layer and exchanges angular momentum with the magnetic moments, producing a spin-orbit torque. The physical origins of the spin Hall effect include three mechanisms: skew scattering, side jump, and Berry curvature in the band (Sinova et al., 2015). Skew scattering and side jump are extrinsic contributions caused by impurity scattering, while Berry curvature is an intrinsic property determined by the band structure (Figure 1).

In the process of impurity scattering, SOC leads to an asymmetry in the scattering probabilities, $W_{kk'} \neq W_{k'k}$, resulting in a preferential deflection of electrons with different spins in opposite directions, a phenomenon known as skew scattering. During impurity scattering, in addition to the deflection of electron momentum, the electron wavepacket also undergo a positional shift. Under an external electric field, the positional shift leads to a change in the kinetic energy of the electron, affecting the transverse current. This process is called side jump. Apart from these impurity-related mechanisms, the spin Berry curvature in the material's band structure act as a gauge field in reciprocal space, causing electrons with opposite spin orientations to deflect in different directions, producing an intrinsic spin current contribution (Xiao et al., 2010).

The total spin Hall conductivity σ_{SH} in a system can be written as the sum of the contributions from the three mechanisms: $\sigma_{SH} = \sigma_{SH}^{int} + \sigma_{SH}^{sk} + \sigma_{SH}^{sj}$. The skew scattering contribution σ_{SH}^{sk} is proportional to the electron relaxation time τ and positively correlated with the material's conductivity, while the side jump (σ_{SH}^{sj}) and intrinsic (σ_{SH}^{int}) contributions are independent of the relaxation time and conductivity. Therefore, the contribution of skew scattering to the spin Hall effect can be inferred by measuring the relationship between σ_{SH} and the conductivity of the material, but it only dominates when the relaxation time is very large, i.e., when the material has excellent conductivity. The intrinsic contribution from the band structure can be obtained through first-principles calculations without relying on impurity scattering and can be compared with experimental results. The spin Hall effect also has a corresponding inverse effect, called the inverse spin Hall effect, which converts spin current into charge current and generally used as a means to detect spin current.

Studies have shown that transition metal oxides, especially 4*d* and 5*d* materials, exhibit significant intrinsic spin Hall effects that are consistent with experimental results (Itoh et al., 2016; Jadaun et al., 2020). This is related to the strong SOC provided by the heavy metal elements in 4*d* and 5*d* materials and is also closely related to the novel electronic structures in them. As mentioned above, when bands of different orbitals overlap, such as the Weyl point, Dirac point/nodal line structures in topological semimetals, they can contribute large spin Berry curvature. Therefore, by changing the crystal field splitting, crystal structure, electron correlation strength, and other factors, targeted regulation can be carried out to achieve the enhancement of the intrinsic spin Hall effect (Jadaun et al., 2020). The coupling of multiple degrees of freedom in transition metal oxides provides a good platform for regulating and enhancing the spin Hall effect.

2.2.2 Rashba-Edelstein effect

In topological surface states and Rashba surface states, the spin-momentum locking property causes electronic states with opposite momenta to have opposite spin orientations at the Fermi surface. When a charge current passes through these surface states, the number of electrons with momenta in the same direction as the charge current increases, leading to an imbalance in the originally dynamically balanced spin electron numbers, resulting in spin accumulation (Figure 1). This phenomenon is called the Rashba-Edelstein effect (Manchon et al., 2015). The resulting spin accumulation can diffuse into the neighboring magnetic layer and interact with the magnetic moments to produce a spin-orbit torque.

Conversely, if a perpendicular spin current is injected into the surface states, spin accumulation will occur at the surface. Due to spin-momentum locking, the spin accumulation will cause asymmetric scattering between electrons with opposite momenta and spins, resulting in a greater number of electrons with momenta locked to the direction of spin accumulation, thus leading to a conversion from spin to charge. This process is called the inverse Rashba-Edelstein effect or spin galvanic effect and can be used to detect spin current at interfaces/surfaces.

The Rashba-Edelstein effect and its inverse process provide a mechanism for efficient interconversion between charge and spin currents in materials with strong spin-orbit coupling and broken inversion symmetry. The spin-momentum locking property of topological and Rashba surface states plays a crucial role in enabling this interconversion, making these states promising candidates for spintronic applications.

2.2.3 Nonlinear effects

The mechanisms described above reflect the charge-spin interconversion that is generated from the electronic structure of the material and exhibits a linear response relationship with the charge current (or electric field E) (Manchon et al., 2019). However, in some novel quantum state materials, such as non-centrosymmetric transition metal chalcogenides, topological Dirac semimetals, 2D Rashba-Dresselhaus systems, etc., there also exists a quadratic response of charge current (J_c) and spin current (J_s) to the electric field, i.e., $J_c, J_s \propto E^2$ (Sodemann and Fu, 2015; He et al., 2018a; He et al., 2018b; Ma et al., 2018; He et al., 2019). Specifically, under the action of an electric field, electrons in non-trivial band structures exhibit a new non-equilibrium distribution. For the Berry curvature, the integral of this non-equilibrium state with respect to the first-order electric field is finite, equivalent to an effective magnetic field caused by the coupling of the Berry curvature under the second-order electric field. This results in a transverse charge current without applying an external magnetic field, known as the quantum nonlinear Hall effect (Sodemann and Fu, 2015; Ma et al., 2018). Similarly, in non-trivial surface states, the non-equilibrium state caused by the second-order electric field also produces a spin current (He et al., 2018b). When an external magnetic field is applied, it causes asymmetric distortion of the surface state contour, and a portion of the spin current can be converted into a charge current in the in-plane direction perpendicular to the magnetic field (Figure 1). resulting in the nonlinear planar Hall effect (He et al., 2019). These novel spin transport-related nonlinear responses can serve as powerful probes to characterize non-trivial electronic structures and also have the potential to expand the functionality of spintronic devices. As a result, they have gradually gained attention in the field of spintronics in recent years. The exploration of nonlinear effects in transition metal oxides with strong SOC and unique electronic structures may lead to the discovery of new phenomena and the development of advanced spintronic applications.

3 Transition metal oxide material systems

When a charge current enters the spin source material, a portion of the charge current is converted into a spin current under the action of the charge-spin interconversion mechanism. The spin current passes through the interface into the neighboring magnetic material and exchanges angular momentum with the magnetic moments, producing a spin-orbit torque (SOT), including the damping-like torque $\sim m \times [m \times (n \times j_c)]$ and field-like torque $\sim m \times (n \times j_c)$ components (Berger, 1996; Slonczewski, 1996; Zhang et al., 2002), where m is the direction of the magnetic moment, n is the interface normal, and j_c is the direction of the charge current. Under the joint action of the two torque components, the originally stable magnetic moment undergoes precession and deviates from the equilibrium position in the direction of the spin polarization. The damping-like torque is mainly responsible for overcoming the magnetic damping to achieve magnetization switching, while the field-like torque is closely related to the dynamics during the magnetization switching process (Katine et al., 2000; Legrand et al., 2015; Yoon et al., 2017; Liu et al., 2021a). The strength of the generated SOT under per unit charge current is one of the key indicators determining the performance of SOT devices. Therefore, quantitatively analyzing the degree of interconversion between charge current and spin current, i.e., the charge-spin conversion efficiency η (including damping-like efficiency η_{DL} and field-like efficiency η_{FL}), is an important basis for evaluating the performance of spin source materials.

Recent discoveries of novel quantum states in TMOs have opened up exciting possibilities for their use as high-performance spin source materials. These quantum states exhibit a strong correlation with charge-spin interconversion and offer a high degree of tunability. To unlock the full potential of TMOs as high-performance spin source materials, researchers are exploring two key strategies: the application of external electric fields and structural engineering techniques. External electric fields can be used to modulate the spin-orbit torque and control the efficiency and direction of charge-spin conversion in TMOs by influencing factors such as charge density, surface states, and SOC (Lesne et al., 2016; Ben Shalom et al., 2010; Caviglia et al., 2010; Vaz et al., 2019; Kaneta-Takada et al., 2022; Noël et al., 2020; Grezes et al., 2023; Gallego et al., 2024). In addition to external electric fields, structural engineering provides another powerful tool for enhancing charge-spin conversion efficiency in TMOs. Structural engineering techniques, including the control of oxygen octahedral rotations, strain engineering, crystal orientation selection, interface engineering, and thickness control, can be employed to precisely design the microscopic structure of TMOs and optimize their charge-spin conversion efficiency (Everhardt et al., 2019; Liu et al., 2019; Nan et al., 2019; Ou et al., 2019; Wang et al., 2019; Huang et al., 2021; Wei et al., 2021; Zhou et al., 2021; Lao et al., 2022; Liu et al., 2022; Zhang et al., 2022; Li et al., 2023; Zhang et al., 2023; Zhang et al., 2024; Zhao et al., 2024).

Spintronic devices based on charge-spin interconversion offer several compelling advantages for information storage, transmission, and processing, including non-volatility, high storage density, low power consumption, and fast response time. Researchers are exploring the use of spin-transfer torque (STT) and SOT to drive magnetization switching and achieve high-performance spintronic devices. Current-induced SOT has emerged as a promising, energy-efficient approach for next-generation spintronic devices (Figure 1). TMOs have garnered significant attention as spin source materials due to their remarkable and highly tunable charge-spin conversion efficiency, making them an ideal platform for spintronic applications. While TMOs have demonstrated efficient control of magnetic materials through SOT, achieving deterministic switching at room temperature without external magnetic fields remains a challenge. Recent breakthroughs in TMO-based SOT devices have shown promising results, but further research is needed to investigate and optimize field-free switching for practical spintronic applications (Liu et al., 2019; Liu et al., 2022; Li et al., 2023; Zhao et al., 2024; Tang et al., 2022).

In the following section, we will introduce promising spin source materials from the perovskite family, including 3*d*-$SrTiO_3$, 4*d*-$SrRuO_3$, 5*d*-$SrIrO_3$ and $KTaO_3$. We will explore the novel quantum states in their electronic structures, which are closely related to SOC and highly sensitive to various degrees of freedom. Furthermore, we will discuss the spin transport mechanisms in these TMOs and the control and enhancement of charge-spin interconversion achieved through diverse approaches. Finally, we will highlight the prospects for their application in high-performance spintronic devices.

3.1 3*d* transition metal oxides: strontium titanate

3*d* transition metal oxides have strong electron correlations and exhibit rich magnetoelectric properties, including metal-insulator transition, magnetism, ferroelectricity, superconductivity, etc. (Imada et al., 1998). Among these materials, strontium titanate ($SrTiO_3$) stands out as a star material, possessing a series of remarkable physical properties (Pai et al., 2018). In bulk $SrTiO_3$, the titanium ions have a $3d^0$ electronic configuration, with the unoccupied 3*d* orbitals forming the bottom of the conduction band. These 3*d* orbitals are separated by a substantial energy gap of approximately 3 *eV* from the O-2*p* orbitals, which constitute the top of the valence band. Consequently $SrTiO_3$ exhibits the characteristics of a wide-bandgap insulator (van Benthem et al., 2001). Under the influence of the crystal field, the 3*d* orbitals undergo degeneracy lifting and split into doubly degenerate e_g and triply degenerate t_{2g} orbitals, with the t_{2g} orbitals located at the bottom of the conduction band. Remarkably, at the surface and heterointerface of $SrTiO_3$, the interplay of band bending and electron doping, caused by charge transfer or oxygen vacancies, leads to the confinement of electrons within a two-dimensional region of several nanometers perpendicular to the surface/interface, giving rising to a highly conductive two-dimensional electron gas (2DEG) (Ohtomo and Hwang, 2004; Stemmer and James Allen, 2014). This 2DEG exhibits excellently controllable magnetoelectric transport properties, superconductivity, quantum Hall effect and other intriguing properties (Reyren et al., 2007; Trier et al., 2016). In recent years, it has been discovered that the 2DEG in $SrTiO_3$ has a special two-dimensional electronic band structure due to the breaking of spatial inversion symmetry at the surface/interface, and exhibits significant charge-spin interconversion capability, attracting wide attention in the field of spintronics.

The electronic structure of bulk insulating $SrTiO_3$ undergoes changes at the surface/interface due to the influence of energy discontinuity and changes in the valence state, leading to the emergence of novel electronic properties that are distinct from those of the bulk material. The originally unoccupied d_{xy}, d_{xz}, and d_{yz} bands within the t_{2g} orbitals descend below the Fermi level, then electrons populate these bands to form a 2DEG. Moreover, the quantum confinement effect induces additional splitting of these bands, yielding sub-bands and manifesting in complex surface electronic structures. King et al. (2014) confirmed the existence of these complex bands through ARPES measurements of the surface electronic structure of $SrTiO_3$. They discovered that when the d_{xy}, d_{xz}, and d_{yz} orbitals are occupied separately, the orbital angular momentum is nearly zero; however, when these bands intersect, the mixed orbitals exhibit significant orbital angular momentum values, contributing to enhanced splitting. Vaz et al. (2019) found that the interface Rashba effect further locks the electrons in the bands into a spin-momentum locked state. Moreover, they pointed out that at certain band crossings, band inversion and non-trivial topological states emerge, resulting in enhanced spin splitting. This pronounced spin splitting, originating from non-trivial electronic structures, directly influences the spin transport behavior through the Rashba-Edelstein effect and inverse Rashba-Edelstein effect, endowing the $SrTiO_3$ surface 2DEG with highly efficient charge-spin interconversion. Besides. Wang et al. (2014) showed that a 2DEG can also be induced at $SrTiO_3$(110) surface. They employed ARPES to achieve a comprehensive photoelectric imaging of the electronic structure of $SrTiO_3$, revealing the complexity of the Fermi surface. As illustrated in Figure 2A, the ellipsoids represent the spatial distribution of different electronic states, with the brighter regions corresponding to the d_{yz}, d_{zx} orbitals, and the darker regions to the d_{xy} orbital. Further measurements of the Fermi surface, as shown in Figure 2B, have uncovered a strong anisotropy in the electronic structure, which significantly differs from the 2DEG oriented along the (001) direction. The capability to achieve a completely flat band suggests favorable prospects for applications in fields such as magnetism and thermoelectricity.

In view of the novel spin configurations exhibited by the $SrTiO_3$ 2DEG, its charge-spin interconversion properties have attracted great interest. Lesne et al. (2016) observed the inverse Rashba-Edelstein effect in the $SrTiO_3/LaAlO_3$ interface 2DEG by SP-FMR method at room temperature, quantifying the two-dimensional charge-spin conversion efficiency of the interface as $\lambda_{IEE} = J_c^{2D} / J_s^{3D} = 6.4\,\mathrm{nm}$. Recently. Kaneta-Takada et al. (2022) observed an even higher conversion efficiency at the $SrTiO_3/LaTiO_{3+\delta}$ interface, $\lambda_{IEE} \sim 190\,\mathrm{nm}$, which was attributed to the joint action of Coulomb repulsion in $LaTiO_{3+\delta}$ and the huge Rashba effect at the interface. Simultaneously, investigations utilizing the Rashba-Edelstein effect as a means of charge-to-spin conversion have also confirmed the significant performance of the $SrTiO_3$ 2DEG. Wang et al. (2017) achieved a remarkable conversion efficiency of 6.3 at room temperature in the heterostructure of $SrTiO_3/LaAlO_3$ and CoFeB. Through variable temperature measurements, they observed a rapid decrease in conversion efficiency with decreasing temperature, ascribing this behavior to the tunneling effect of electrons in localized states within $LaAlO_3$. In addition to the Rashba-Edelstein effect, other mechanisms of charge-spin interconversion have been explored in the $SrTiO_3$ 2DEG system. Sinova et al. (2004) theoretically predicted the presence of a two-dimensional spin Hall effect at the Rashba interface, presenting another mechanism for interface charge-spin interconversion. The spin current generated by this effect is in-plane and perpendicular to the current, with the spin polarization perpendicular to the interface. Experimentally. Jin et al. (2017) and Trier et al. (2020) et al. detected the electrical signals generated by the two-dimensional spin Hall effect and inverse spin Hall effect at the $SrTiO_3/LaAlO_3$ interface through non-local transport measurements (Figure 2C). Furthermore, the nonlinear magnetoresistance effect can be employed to enhance the detection and manipulation capabilities of spin currents. He et al. (2018a) reported the observation of gate-tunable bilinear magnetoelectric resistance (BMER) signals on Ar^+ irradiated conductive $SrTiO_3$ surfaces (Figure 2D). In addition to the conventional in-plane spin component perpendicular to the momentum locking, the BMER measurement results indicate that the 2DEG possesses an unconventional threefold symmetric out-of-plane spin component, consistent with tight-binding calculations. Notably, this unconventional spin current can generate SOT, breaking the mirror symmetry of perpendicular magnetization, and holds promise for achieving field-free magnetization switching.

Building upon these findings. Lesne et al. (2016) not only measured a large charge-spin interconversion efficiency at the $SrTiO_3/LaAlO_3$ interface but also demonstrated the ability to tune the conversion efficiency at the interface using gate voltage. This voltage-driven tunability was previously observed by Ben Shalom et al. (2010) and Caviglia et al. (2010), who found that applying an external voltage enables effective modulation of the charge-spin interconversion. These discoveries underscore the potential for highly efficient and flexibly tunable performance in spintronic devices based on the $SrTiO_3$ surface 2DEG. Vaz et al. (2019) observed the corresponding change of λ_{IEE} (Figure 2E) by voltage regulation of the Fermi surface position of the $SrTiO_3$/Al interface, with a maximum value of 28 nm. This high tunability by voltage is the result of the non-trivial band structure mentioned above. When the Fermi surface moves to the band crossing under a certain voltage, electrons will undergo more charge-spin interconversion through spin-momentum locking, thus enhancing the conversion efficiency. In addition, using the ferroelectricity of $SrTiO_3$ at low temperatures. Noël et al. (2020) demonstrated that the sign of spin-charge conversion can be non-volatilely regulated by an electric field. Similarly. Grezes et al. (2023) also presented results in a CoFeB/MgO heterostructure on $SrTiO_3$. By adjusting the back-gate voltage, they precisely controlled the 2DEG electron filling state and Fermi level, thereby altering the amplitude and sign of the SOT (Figure 2F), achieving non-volatile electric field control of SOT in the 2DEG based on the Rashba-Edelstein effect. To date, spin-charge interconversion in the 2DEG of $SrTiO_3$ has been primarily achieved through spin pumping. To further exploit its potential in spin-orbit electronic devices, it is necessary to realize direct electrical spin injection in nanoscale

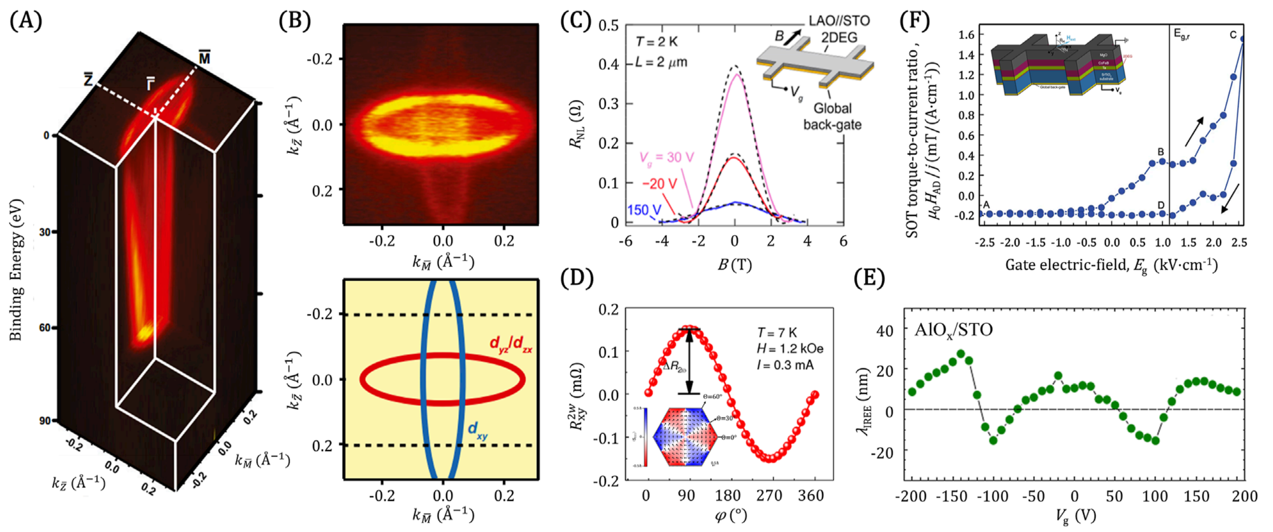

FIGURE 2
Electronic structure and charge-spin interconversion in the 2DEG at the surface/interface of $SrTiO_3$: **(A)** Full photoemission mapping and **(B)** constant energy cuts and schematic constant-energy surfaces of the $SrTiO_3$ 2DEG measured by ARPES (Adapted with permission from Ref (Wang et al., 2014).); **(C)** Measurement of the spin Hall effect and inverse spin Hall effect in the 2DEG through nonlocal transport, and the voltage-controlled Hanle effect can be observed by applying an external magnetic field (Reproduced with permission from Ref (Trier et al., 2020).); **(D)** Angular dependence of the second harmonic planar Hall resistance R_{2w} of $SrTiO_3$(111) surface, with the inset showing the spin texture of the Fermi surface (Adapted with permission from Ref (He et al., 2018a).); **(E)** Variation of the charge-spin conversion efficiency λ_{IEE} of the $SrTiO_3$ 2DEG with control voltage V_g (Reproduced with permission from Ref (To et al., 2021).); **(F)** Gate field dependence of the spin-orbit torque and anti-damping-like effective field, with the inset showing a schematic diagram of the measurement configuration for charge-spin conversion in the MgO/CoFeB/Ta/STO device (Adapted with permission from Ref (Grezes et al., 2023).).

devices. Gallego et al. (2024) designed a nanodevice based on the $SrTiO_3/LaAlO_3$ interface 2DEG, performing all-electrical spin injection based on the inverse Edelstein effect. By optimizing the spin-charge conversion efficiency through back-gate voltage, they obtained a two-dimensional charge-spin conversion efficiency λ_{IEE} of 0.72 nm for this interface at 2 K. In addition to voltage control, the regulation of charge-spin interconversion by the interface electronic structure is also crucial. Zhang et al. (2022) achieved a charge-spin interconversion efficiency as high as approximately 2.4 at room temperature by precisely controlling the thickness of the $LaTiO_{3+\delta}$ layer at the $SrTiO_3/LaTiO_{3+\delta}$ interface. Moreover, the conversion efficiency exhibited stability with temperature variation, indicating its immense potential in developing low-power, high-efficiency spintronic devices.

The aforementioned research results confirm that the $SrTiO_3$ interface 2DEG possesses significant and highly tunable charge-spin interconversion, which can be closely related to its novel electronic structure. In particular, the huge conversion efficiency recently observed at the $SrTiO_3/LaTiO_{3+\delta}$ interface indicates that the SOT properties of the 2DEG system still have great room for enhancement. In view of the intricate physical mechanisms involved, how to profoundly understand the influence of non-trivial electronic structures on charge-spin interconversion, and how to induce, characterize, and utilize novel topological states in a targeted manner to improve conversion efficiency are important research directions. It is noteworthy that current work primarily focuses on characterizing the charge-spin conversion efficiency. Given the enormous application potential of the $SrTiO_3$ system, future research should place more emphasis on SOT manipulation of magnetization switching and developing functional spintronic devices.

3.2 *4d* transition metal oxides: Strontium ruthenate

4d transition metal oxides have attracted much attention due to their relatively strong correlation effects, moderate SOC strength, and the interaction between the crystal field environment. The strontium ruthenate family, $Sr_{n+1}Ru_nO_{3n+1}$, is a prime example of these materials, with each member exhibiting unique properties. $Sr_3Ru_2O_7$ has novel metamagnetism (Grigera et al., 2004), while Sr_2RuO_4 exhibits unconventional *p*-wave superconductivity (Luke et al., 1998). Among the family, $SrRuO_3$ stands out for its itinerant ferromagnetism, strong magnetic anisotropy, good thermal stability, chemical stability, conductivity. These characteristics has motivated a large number of fundamental studies to explore the evolution of $SrRuO_3$'s magnetoelectric properties through means such as strain, doping, and dimensionality. Moreover, $SrRuO_3$ has been applied as an electrode material in various magnetoelectric devices, including field effect transistors, ferroelectric capacitors, magnetic tunnel junctions (Koster et al., 2012). In recent years, researchers have found that $SrRuO_3$ possesses spin transport properties related to novel electronic structures, further increasing its appeal in the field of spintronics. The combination of its unique properties and the potential for spintronic applications has positioned $SrRuO_3$ as a material of great interest for both fundamental research and practical applications.

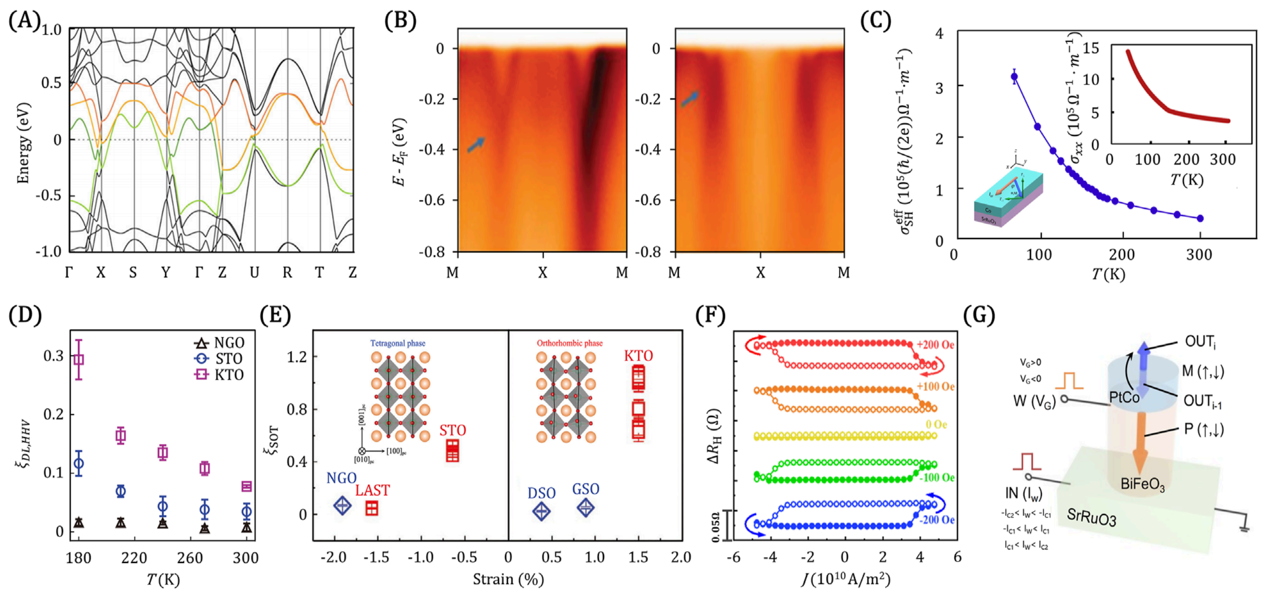

FIGURE 3
Electronic structures, spin transport properties and SOT associated characterization results of $SrRuO_3$: **(A)** Band structure of $SrRuO_3$ based on GGA calculations, considering the effects of magnetism, SOC and Coulomb interaction (Reproduced with permission from Ref (Takiguchi et al., 2020).); **(B)** Energy momentum mappings for $SrRuO_3$(001) measured by ARPES. The Wely point are indicated with arrows (Reproduced with permission from Ref (Lin et al., 2021).); **(C)** Spin Hall conductivity of $SrRuO_3$ as a function of temperature ranging from 300 to 60 K (inset: the corresponding electrical conductivity in the same temperature range) (Adapted with permission from Ref (Ou et al., 2019).); **(D)** Charge-spin conversion efficiency of $SrRuO_3$ grown on various substrates as a function of temperature (Reproduced with permission from Ref (Zhou et al., 2021).); **(E)** Comparison of charge-spin conversion efficiency between orthorhombic (red square) and tetragonal (blue diamond) $SrRuO_3$ grown on various substrates (Adapted with permission from Ref (Wei et al., 2021).); **(F)** Magnetization switching driven by pulse current under different external magnetic fields H_x (Reproduced with permission from Ref (Li et al., 2023).); **(G)** Schematic diagram of multiferroic magnonic spin torque logic with a single storage unit placed on the spin current channel (Adapted with permission from Ref (Chai et al., 2023).).

Theoretical calculations predict that the band structure of $SrRuO_3$ has multiple linear dispersive band crossing points near the Fermi surface, as shown in Figure 3A. These configurations, composed of t_{2g} orbitals and closely related to topological non-triviality, can provide significant Berry curvature (Fang et al., 2003; Mathieu et al., 2004), which is a key factor in the generation of novel quantum states in $SrRuO_3$. Chen et al. (2013) predicted the existence of a large number of magnetic topological Weyl points in the electronic structure of $SrRuO_3$ after considering the influence of magnetism and SOC, and the Berry curvature in them makes it possess significant intrinsic anomalous Hall effect. Experimental studies have provided evidence for the predicted novel electronic structure and spin transport properties of $SrRuO_3$. Takiguchi et al. (2020) observed quantum transport phenomena, including linear positive magnetoresistance and chiral anomaly, caused by Berry curvature through low-temperature magnetoelectric transport measurements. Lin et al. (2021) characterized the electronic band structure of $SrRuO_3$ by ARPES, and combined with first-principles calculations, confirming the existence of Weyl points near the Fermi surface (Figure 3B). They found that its anomalous Hall conductivity exhibits a non-monotonic evolution under the action of an external electric field. Tian et al. (2021) demonstrate the tuning of the anomalous Hall effect through strain engineering and confirmed its origin in the change of Berry curvature. These results confirm that $SrRuO_3$ possesses novel and highly tunable band structures and topological quantum states, which provide significant Berry curvature and exhibit related spin transport characteristics.

The Berry curvature in the electronic bands of $SrRuO_3$ not only contributes to the intrinsic anomalous Hall effect, but can also produce the spin Hall effect, thus bringing significant charge-spin interconversion. Haidar et al. (2015) measured the voltage signal generated by $SrTiO_3$(001)/$La_{0.67}Sr_{0.33}MnO_3$(LSMO)/$SrRuO_3$ at room temperature by the spin pumping-ferromagnetic resonance (SP-FMR) method. They found a component that has a $\cos\varphi$ relationship with the magnetic field and increases significantly with the input power, attributing its source to the inverse spin Hall effect with LSMO as the spin pumping source. Similar SP-FMR results (Richter et al., 2017) were also confirmed in $Y_3Fe_5O_{12}$/$SrRuO_3$ grown on $Gd_3Ga_5O_{12}$(111). These results demonstrate that the spin current generated by the magnetic oxide is converted into charge current through $SrRuO_3$, confirming that its spin-charge interconversion capability. Wahler et al. (2016) also observed similar SP-FMR results in $NdGaO_3$(110)/LSMO/$SrRuO_3$ and quantitatively gave the spin transport-related parameters of $SrRuO_3$, such as spin diffusion constant $\lambda \sim 1.5$ nm and conversion efficiency $\eta \sim 0.03$. By varying the measurement temperature, they found that the inverse spin Hall voltage shows a monotonic decreasing trend below the Curie temperature of $SrRuO_3$ (~160 K), revealing that the magnetism of $SrRuO_3$ affects its charge-spin conversion efficiency.

The above studies demonstrate well the picture that the novel electronic structure of $SrRuO_3$ is the source of its spin transport properties. However, compared to the large Berry curvature reflected by the anomalous Hall effect, the Berry curvature reflected by the inverse spin Hall effect is not significant. This contradiction is most likely due to the inevitable parasitic rectification effect in the SP-FMR experiment leading to an underestimation of the inverse spin Hall voltage (Mosendz et al., 2010). Therefore, recent related work has focused on characterizing the SOT generated by the spin Hall effect of $SrRuO_3$ to more accurately and deeply investigate its charge-spin interconversion. Ou et al. (2019) systematically characterized the spin Hall conductivity in Si/$SrTiO_3$/$SrRuO_3$/Co by the spin torque-ferromagnetic resonance (ST-FMR) method. As shown in Figure 3C, the spin Hall conductivity shows a monotonic increase in the temperature range from 300 K to 60 K, up to 3×10^5 $(\hbar/(2e))\Omega^{-1}\mathrm{m}^{-1}$, equivalent to a conversion efficiency of η ~ 0.3. Notably, the spin Hall conductivity and conductivity show a very consistent trend with temperature, maintaining the original trend on both sides of the Curie temperature of $SrRuO_3$. Ou et al. (2019). suggest that this charge-spin interconversion property, which is almost unaffected by magnetism, may originate from the intrinsic spin Hall effect. Tang et al. (2022) used the harmonic Hall voltage (HHV) method to measure the SOT efficiency of $SrTiO_3$/$SrRuO_3$/FeGd, obtaining a value of 0.04. The lower SOT efficiency may be due to the lower interfacial spin transmission between the oxide and the ferromagnetic FeGd, which requires further investigation. Recently. Li et al. (2023) systematically measured the SOT efficiency of $SrRuO_3$ (001) thin films in heterostructures with in-plane magnetic anisotropy (IMA) and perpendicular magnetic anisotropy (PMA) materials at room temperature, obtaining a value of approximately 0.2, comparable to that of heavy metals. This value serves as a reference for future studies on SOT efficiency in $SrRuO_3$.

In addition to discussing the charge-spin conversion. Ou et al. (2019) also observed a vertical spin polarization component below the Curie temperature and pointed out that it may be related to the strong anisotropic magnetoresistance of $SrRuO_3$. Moreover, combined with the characterization results of the crystal structure, they found that the spin Hall effect strength of $SrRuO_3$ is closely related to the degree of rotation of the RuO_6 oxygen octahedra, suggesting that enhanced conversion efficiency could be achieved through structural regulation. Recently. Zhou et al. (2021) and Wei et al. (2021) systematically studied the evolution of the SOT-related properties of $SrRuO_3$ under different strain and crystal structures by regulating the crystal structure of $SrRuO_3$ through epitaxial strain. They found that by applying −1.9% to +1.5% epitaxial strain to $SrRuO_3$ through varying a series of substrates, its crystal structure undergoes changes in the tetragonal and orthorhombic phases, greatly affecting its charge-spin conversion efficiency. In the work of Zhou et al. (2021), as shown in Figure 3D, under different strain states, the conversion efficiency of $SrRuO_3$ increases monotonically with decreasing temperature, indicating that the intrinsic spin Hall effect is the main contribution source, combined with the measurement of the change in conductivity. When the $SrRuO_3$ thin films are grown on $NdGaO_3$ substrates, the RuO_6 octahedra only rotate out-of-plane, resulting in a tetragonal crystal structure with a conversion efficiency of η ~ 0.01. In contrast, when grown on $SrTiO_3$ and $KTaO_3$ substrates, the RuO_6 octahedra rotate both in-plane and out-of-plane, leading to an orthorhombic structure with a larger conversion efficiency of η ~ 0.1–0.3. The same trend is also observed in the work of Wei et al. (2021). As shown in Figure 3E, compared to the conversion efficiency of η ~ 0.05 for the tetragonal $SrRuO_3$ (blue diamonds), the orthorhombic $SrRuO_3$ (red squares) shows a very significant increase in conversion efficiency, reaching up to η ~ 1 depending on the strain. This result indicates that by structurally regulating the crystal field distortion, the arrangement of e_g and t_{2g} electron orbitals can be directly affected, enabling the tuning of the electronic band structure and Berry curvature. Furthermore, crystal orientation is also an important means to regulate the properties of TMO materials. Zhao et al. (2024) systematically explored the influence of crystal orientation on the SOT properties of $SrRuO_3$/CoPt heterostructures and found that the SOT efficiency of (111)-oriented $SrRuO_3$ reaches 0.39, nearly twice that of (001)-oriented $SrRuO_3$, with the spin Hall conductivity also increasing by nearly an order of magnitude. This demonstrates that crystal plane orientation control is an effective strategy for optimizing SOT and provides new ideas for further improving the performance of spintronic devices.

$SrRuO_3$ exhibits significant and highly tunable charge-spin conversion efficiency, and further utilizing the generated SOT to drive magnetization switching is a key step for spin-based data storage and logic. Tang et al. (2022) designed an $SrRuO_3$/FeGd heterostructure and achieved SOT-driven magnetization switching at room temperature with a low threshold current density of 4.5×10^6 A/cm^2 under a small in-plane magnetic field, which is smaller than the switching current in heavy metal/ferromagnet bilayers (usually on the order of 10^7 A/cm^2). Recently, Li et al. (2023) also realized SOT-driven magnetization switching in $SrRuO_3$/CoPt devices at room temperature (Figure 3F), with a switching threshold current density of 3.8×10^6 A/cm^2. After continuously applying pulses larger than the switching current, they found that the devices exhibit highly repeatable SOT-driven responses, demonstrating the repeatability and stability of magnetization switching in $SrRuO_3$. Similarly, Zhao et al. (2024) also achieved magnetization switching in $SrRuO_3$/CoPt with a threshold current density of 2.4×10^6 A/cm^2, and the slight difference in threshold current density may be due to different crystal orientations. These results demonstrate the feasibility of using $SrRuO_3$ for energy-efficient SOT applications.

Furthermore, Chai et al., (2023) designed a magnon-mediated spin torque (MST) device by constructing an $SrRuO_3$/$BiFeO_3$/CoPt multilayer heterostructure, demonstrating effective spin transmission and magnetization switching. By applying current pulses to the $SrRuO_3$ layer, spin accumulation is generated at the interface, exciting magneton modes in $BiFeO_3$. When the magnons transmit to the CoPt layer, the magnetization direction is controlled through magnon-mediated spin torque (MST), realizing parallel non-volatile writing of multiple storage units. As shown in Figure 3G, by applying different V_{G} and I_w, different logic functions can be achieved. When the ferroelectric polarization direction is upward ($W = 1$), the intermediate current I_w ($-I_{c2} < I_w < -I_{c1}$ or $I_{c1} < I_w < I_{c2}$) switches the output magnetization state. Smaller I_w ($-I_{c1} < I_w < I_{c1}$) maintains the initial magnetization state ($OUT_i = OUT_{i-1}$). By presetting the initial state OUT_{i-1} and defining IN, a complete set of logic functions can be realized and reconfigured. Multiferroic magnon spin torque technology combines the magnetoelectric properties of multiferroic materials and spin torque effects, providing new possibilities for developing next-generation storage devices and artificial intelligence.

The above SOT results confirm that $SrRuO_3$ possesses significant Berry curvature and strong spin Hall effect, and can achieve efficient charge-spin interconversion. Further regulating the electronic structure of $SrRuO_3$ through strain engineering greatly enhances its charge-spin conversion efficiency, surpassing traditional heavy metals. In addition, considering that $SrRuO_3$ also possesses excellent thermal stability, chemical stability, and high conductivity, as well as good compatibility with magnetic metals and oxides, it is a very promising spin source material. However, regarding the efficiency of $SrRuO_3$'s charge-spin interconversion and its evolution with temperature, there are still some divergences at present. First, by comparing the results of Wahler et al. (2016) and Ou et al. (2019), it can be seen that in the non-magnetic temperature range, the spin Hall effect-related parameters of $SrRuO_3$ increase with decreasing temperature, showing a consistent trend. However, below the Curie temperature (160 K), Wahler et al. observed a sharp decrease in the inverse spin Hall voltage, while Ou et al. found a continued increase in the spin Hall conductivity. This contradictory result concerns the influence of $SrRuO_3$'s magnetism on its charge-spin interconversion capability, and needs to be further confirmed, with its underlying physical mechanism clarified. Second, although it is currently widely accepted that the source of $SrRuO_3$'s efficient charge-spin interconversion is the significant Berry curvature brought about by its electronic band structure, there are still large discrepancies in the specific charge-spin conversion efficiency values. As shown in Table 1, in the same $SrTiO_3$(001)/$SrRuO_3$/Py structure, although there are some slight differences in the thickness of each layer, the conversion efficiency η observed in different works (Wei et al., 2021; Zhou et al., 2021) differs by an order of magnitude, ranging from 0.04 to 0.5. Therefore, it is necessary to accurately measure the charge-spin interconversion efficiency of $SrRuO_3$. Finally, although $SrRuO_3$ exhibits significant and highly tunable charge-spin conversion efficiency, reports on using the SOT it generates to drive magnetization switching are still very limited, and key parameters such as the switching threshold current urgently need further exploration.

3.3 5*d* transition metal oxides

3.3.1 Strontium iridate

5*d* transition metal iridium oxides, characterized by strong spin-orbit interaction and moderate electron correlation, are an important material system for realizing and studying correlated topological quantum states. Among various iridium oxides, layered perovskite iridium oxides, such as the Ruddlesden-Popper phase strontium iridates $Sr_{n+1}Ir_nO_{3n+1}$, have attracted substantial attention. Sr_2IrO_4 ($n = 1$), as a typical spin-orbit coupled Mott insulator, is formed by the synergistic interplay of strong spin-orbit interaction and electron correlation (Kim et al., 2008), and possesses a $J_{eff} = 1/2$ single-band structure similar to that of copper-based high-temperature superconductors. As the value of n increases, the structure of $Sr_{n+1}Ir_nO_{3n+1}$ gradually changes from a two-dimensional layered structure to a three-dimensional structure, accompanied by corresponding changes in its physical properties (Moon et al., 2008). For example, $Sr_3Ir_2O_7$ ($n = 2$) transforms into a semiconductor, while $SrIrO_3$ ($n = \infty$) exhibits semimetallic behavior. Currently, a large body of theoretical and experimental studies investigate the presence of novel correlated topological quantum states and SOT-related novel spin transport properties in perovskite-structured $SrIrO_3$.

Theoretical studies predict the existence of a variety of correlated topological quantum states in perovskite-structured $SrIrO_3$ thin films and heterostructures. Carter et al. (2012) employed tight-binding Hamiltonian model calculations to predict the existence of a three-dimensional topological nodal semimetal state in bulk perovskite-structured $SrIrO_3$, which is protected by spin-orbit coupling and lattice symmetry. Kim et al. (2015) predicted the existence of a Dirac fermion state on the $SrIrO_3$ (001) surface, with a non-trivial topological Z_2 index protected by time-reversal symmetry. On the experimental front, Nie et al. (2015) characterized the electronic structure of single-crystal $SrIrO_3$ thin films grown on $((LaAlO_3)_{0.3}(SrAl_{1/2}Ta_{1/2}O_3)_{0.7})$LSAT(001) substrates using *in situ* ARPES and observed the coexistence of electron and hole bands along with significant band renormalization. Intriguingly, the electron band exhibits the possible existence of a Dirac cone-like electronic structure (Figure 4A), in agreement with the theoretically predicted topological nodal semimetal state. In contrast, Liu et al. (2016a) investigated high-quality $SrIrO_3$ thin films grown on $SrTiO_3$(001) substrates using a combined oxide-MBE and ARPES system. By combining ARPES results with first-principles calculations, they suggested that there are signs of a gap opening at the crossing position of the electron bands, which does not support the theoretically predicted topological semimetal state. Further analysis reveals that while maintaining mirror symmetry, the width of the bandgap can be tuned by changing the glide symmetry of the crystal structure, thereby influencing the topological properties of $SrIrO_3$ (Liu et al., 2016b). Moreover, Fujioka et al. (2019) highlighted that the distance between the Dirac node and the Fermi level can be effectively modulated by adjusting the coupling strength of SOC and electron correlation, thus impacting the topological properties of $SrIrO_3$. As non-trivial topological electronic structures are crucial factors for the existence of efficient charge-spin interconversion, the above studies demonstrate, through a combination of theory and experiments, that the electronic structure of $SrIrO_3$ possesses non-trivial and highly tunable topological band properties, rendering it a promising material for efficient charge-spin interconversion.

Regarding spin transport properties, Patri et al. (2018) conducted theoretical calculations on the spin Hall effect of bulk $SrIrO_3$ and found that the combination of strong SOC and the Dirac nodal line band structure give rise to a huge Berry curvature, endowing $SrIrO_3$ with significant intrinsic spin Hall conductivity, which can reach values on the order of 10^4 $(\hbar/(2e))\Omega^{-1}m^{-1}$. Jadaun et al. (2020) further investigated the influence of various intrinsic factors on the spin Hall conductivity of $SrIrO_3$ and concluded that the crystal field strength, crystal structure distortion, Fermi level position, and electron correlation are crucial determinants. Apart from the bulk contribution, Kim et al. (2015) and Chen et al. (2015) demonstrated through theoretical calculations that $SrIrO_3$ harbors non-trivial surface states protected by lattice symmetry, which can facilitate charge-spin interconversion. Lao et al. (2022) observed significantly different spin Hall conductivities along different crystal orientations in $SrIrO_3$(110) thin films, as shown in (Figure 4B), which predominantly influences the magnitude of the damping-like torque efficiency. Concerning charge-spin conversion efficiency,

TABLE 1 Comparison of the SOT-efficiencies and spin Hall conductivity in transition metal oxide systems. λ_{IEE} is the length of the inverse Edelstein effect, and the larger its value, the higher the efficiency of spin-to-charge conversion. η_{DL} is the damping-like SOT-efficiency, ρ_{SOC} is the resistivity of SOC layer, σ_{xy}^{SH} and J_{SW} present the spin Hall conductivity and threshold current density, respectively.

Materials	T [K]	λ_{IEE} [nm]	η_{DL}	J_{SW} [$\times 10^6$ $A \cdot cm^{-2}$]	ρ_{SOC} [$\mu\Omega \cdot cm$]	σ_{xy}^{SH} [$\times 10^2$ $(\hbar/(2e))\Omega^{-1}cm^{-1}$]	Method	Mechanism
Py/Al/STO(001) (Vaz et al., 2019)	15	(+28, −16)					spin-pumping	IEE
Py/Al/STO(001) (Vaz et al., 2019)	RT	0.5 ± 0.1					spin-pumping	IEE
Py/LAO/STO(001) (Lesne et al., 2016)	7	6.4					spin-pumping	IEE
LSMO/LTO/STO(001) (Kaneta-Takada et al., 2022)	15	193.5					spin-pumping	IEE
Py/Al/STO(001) (Noël et al., 2020)	7	±60					spin-pumping	IEE
CoFeB/LAO/STO(001) (Wang et al., 2017)	RT		6.3 ± 1				ST-FMR	REE
LAO/STO (001)(Jin et al., 2017)	2		0.15 ± 0.05				Hanle experiment	SHE、ISHE
LAO/STO(001) (Trier et al., 2020)	2		0.136 ± 0.082				Hanle experiment	ISHE
LAO/STO(111) (He et al., 2018a)	2						Harmonic	BMER
Py/LTO/STO(001) (Zhang et al., 2022)	RT		2.4				ST-FMR	REE
LAO/STO(001) (Gallego et al., 2024)	2	0.72					spin-pumping	IEE
SRO/LSMO/NGO(110) (Wahler et al., 2016)	190		0.027 ± 0.018		156.25–116.28	1.728–2.32	SP-FMR	ISHE
Co/SRO/STO/Si(001) (Ou et al., 2019)	RT		0.1 ± 0.02		250	4	ST-FMR	SHE
Co/SRO/STO/Si(001) (Ou et al., 2019)	60		0.23		71	32	ST-FMR	SHE
Py/SRO/NGO(001) (Zhou et al., 2021)	RT		0.015		114.3	2.6	ST-FMR	SHE
Py/SRO/NGO(001) (Zhou et al., 2021)	RT		0.008		114.3	1.4	Harmonic	SHE
Py/SRO/STO(001) (Zhou et al., 2021)	RT		0.139		120.5	23	ST-FMR	SHE
Py/SRO/STO(001) (Zhou et al., 2021)	RT		0.035		120.5	5.8	Harmonic	SHE
Py/SRO/KTO(001) (Zhou et al., 2021)	RT		0.154		174.7	17.6	ST-FMR	SHE
Py/SRO/KTO(001) (Zhou et al., 2021)	RT		0.078		174.7	8.9	Harmonic	SHE

(Continued on the following page)

TABLE 1 (*Continued*) Comparison of the SOT-efficiencies and spin Hall conductivity in transition metal oxide systems. λ_{IEE} is the length of the inverse Edelstein effect, and the larger its value, the higher the efficiency of spin-to-charge conversion. η_{DL} is the damping-like SOT-efficiency, ρ_{SOC} is the resistivity of SOC layer, σ_{xy}^{SH} and J_{SW} present the spin Hall conductivity and threshold current density, respectively.

Materials	$T[K]$	λ_{IEE} $[nm]$	η_{DL}	$J_{SW}[\times 10^6$ $A \cdot cm^{-2}]$	$\rho_{SOC}[\mu\Omega \cdot$ $cm]$	$\sigma_{xy}^{SH}[\times 10^2$ $(\hbar/(2e))\Omega^{-1}cm^{-1}]$	Method	Mechanism
Py/SRO/STO(001) (Wei et al., 2021)	RT		~0.49		810	5.7	ST-FMR	SHE
Py/SRO/KTO(001) (Wei et al., 2021)	RT		0.89		1,000	8.82	ST-FMR	SHE
Py/SRO/LSAT(001) (Wei et al., 2021)	RT		~0.05		790	0.54	ST-FMR	SHE
Py/SRO/STO(001) (Li et al., 2023)	RT		0.175		156	11.2	Harmonic	SHE
CoPt/SRO/STO(001) (Li et al., 2023)	RT		0.21	3.8	450	4.68	Harmonic	SHE
FeGd/SRO/STO(001) (Tang et al., 2022)	RT		0.04	4.5	160	2.5	Harmonic	SHE
CoPt/SRO/STO(111) (Zhao et al., 2024)	RT		0.39	2.4	178	21.9	Harmonic	SHE
SIO/LSAT(001) (Kozuka et al., 2021)	RT				500		Harmonic	NPHE
SIO/GSO(110) (Kozuka et al., 2021)	RT				470		Harmonic	NPHE
SIO/NGO(110) (Kozuka et al., 2021)	RT				3,300		Harmonic	NPHE
Py/SIO/STO(001) (Nan et al., 2019)	RT		0.51 ± 0.07		400	12.75	ST-FMR	SHE
Py/SIO/LSAT (Everhardt et al., 2019)	RT		0.3–0.5		500	6–10	ST-FMR	SHE
CoFeB/SIO/SRO/STO(001) (Liu et al., 2019)	70			4.6–5.0	110		Harmonic	SHE
CoFeB/SIO/SRO/STO(110) (Liu et al., 2019)	70		0.58–0.86		165	35–52	Harmonic	SHE
CoTb/SIO/STO(001) (Wang et al., 2019)	RT		1.08 ± 0.11		1,200	9	Harmonic	SHE
SIO/LSMO/STO(001) (Huang et al., 2021)	RT		1		1,000–330	10–30	ST-FMR	SHE
SIO/LSMO/NGO(001) (Liu et al., 2022)	RT		0.15	2.9			Harmonic	SHE
FeGd/SIO/STO(001) (Tang et al., 2022)	RT		0.1	3	620	1.61	Harmonic	SHE
Py/SIO/STO(110)-[001] (Lao et al., 2022)	290		0.46		433	10.62	Harmonic	SHE、NPHE
Py/SIO/STO(110)-[1-10] (Lao et al., 2022)	290		0.25		433	5.77	Harmonic	SHE、NPHE
Py/SIO/STO(001) (Zhang et al., 2024a)	RT		1.05		585	17.95	ST-FMR	SHE

(Continued on the following page)

TABLE 1 (*Continued*) Comparison of the SOT-efficiencies and spin Hall conductivity in transition metal oxide systems. λ_{IEE} is the length of the inverse Edelstein effect, and the larger its value, the higher the efficiency of spin-to-charge conversion. η_{DL} is the damping-like SOT-efficiency, ρ_{SOC} is the resistivity of SOC layer, σ_{xy}^{SH} and J_{SW} present the spin Hall conductivity and threshold current density, respectively.

Materials	$T[K]$	λ_{IEE} $[nm]$	η_{DL}	$J_{SW}[\times 10^6$ $A \cdot cm^{-2}]$	$\rho_{SOC}[\mu\Omega \cdot cm]$	$\sigma_{xy}^{SH}[\times 10^2$ $(\hbar/(2e))\Omega^{-1}cm^{-1}]$	Method	Mechanism
Py/SIO/KTO(001) (Zhang et al., 2024a)	RT		1.45		1,047	13.85	ST-FMR	SHE
Py/SIO/NGO(001) (Zhang et al., 2024a)	RT		0.15		2,267	0.66	ST-FMR	SHE
Py/SIO/DSO (Chen et al., 2024)	RT		0.63		4,100	1.54	ST-FMR	SHE
Py/SIO/DSO (Chen et al., 2024)	RT		0.55		4,100	1.34	Harmonic	SHE
Py/Al/KTO(001) (Vicente-Arche et al., 2021)	10	−3.5					SP-FMR	IEE
Py/γ -Al_2O_3/KTO(001) (Zhang et al., 2023)	5		3.6				ST-FMR	REE
Py/γ -Al_2O_3/KTO(001) (Zhang et al., 2023)	300		1.1				ST-FMR	REE

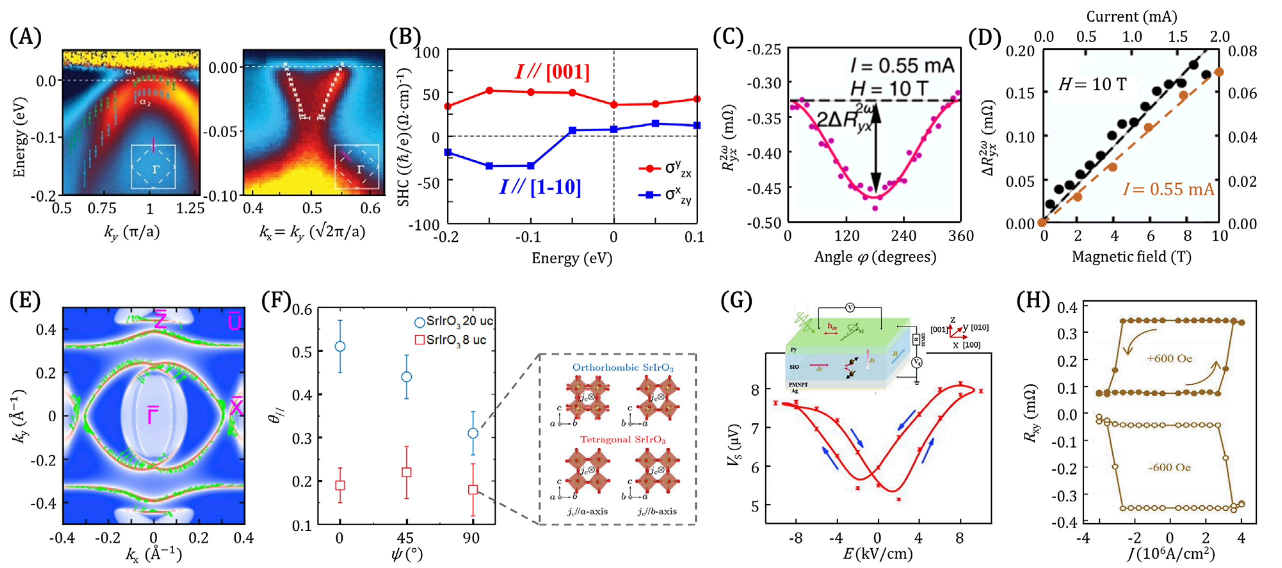

FIGURE 4
Electronic structures, spin transport properties and SOT associated characterization results of $SrIrO_3$: **(A)** The electronic structure map near the Fermi surface measured by ARPES. left: the hole like bands near the Fermi surface. right: the linearly dispersive electron band near the Fermi surface (Reproduced with permission from Ref (Nie et al., 2015).); **(B)** Spin Hall conductivities for current I along the [001] (red circles) and [1-10] (blue squares) directions, respectively. Here, the notation $\sigma_{\alpha\beta}^{y}$ denotes that charge current, spin current, and spin polarization are along β, α, and γ directions, respectively (Reproduced with permission from Ref (Lao et al., 2022).); **(C)** Second-harmonic planar Hall resistance $\Delta R_{yx}^{2w} = V_{yx}^{2w}/I$ as a function of φ and fitting with $\Delta R_{yx}^{2w}\cos\varphi$ (Reproduced with permission from Ref (Kozuka et al., 2021).); **(D)** Current and magnetic field dependences of ΔR_{yx}^{2w} (Adapted with permission from Ref (Kozuka et al., 2021).); **(E)** Fermi surface on the $k_x - k_y$ plane, where the green arrows denote the spin directions (Reproduced with permission from Ref (Lao et al., 2022).); **(F)** Charge-spin conversion efficiency of $SrIrO_3$(001)/Py with orthorhombic and tetragonal structures, the right schematic illustrates side view of the orthorhombic and tetragonal crystalline structures, respectively (Adapted with permission from Ref (Nan et al., 2019).); **(G)** Reversible electric field control of the amplitude of the symmetric spin pumping component V_s, the schematic illustrates the PMN-PT/$SrIrO_3$/Py sample for the inverse spin Hall effect measurement setup with a gate electric field E along the out-of-plane direction of the (001)-oriented (Adapted with permission from Ref (Cui et al., 2021).); **(H)** Current-induced switching behavior of $SrRuO_3$/FeGd with different in-plane magnetic fields at room temperature (Reproduced with permission from Ref (Tang et al., 2022).).

Nan et al. (2019) reported a damping-like torque efficiency of η_{DL} = 0.5 in $SrTiO_3(001)/SrIrO_3/Py$, which exhibits significant variations with crystal orientation and structural phase transitions induced by oxygen octahedral rotation (Figure 4F). Everhardt et al. (2019) found a damping-like torque efficiency ($\eta_{DL} \propto 1/\rho$) inversely correlated with the resistivity of $SrIrO_3$ in $SrIrO_3/Py$ grown on LSAT substrates, and highlighted that this correlation differs from that observed in traditional heavy metal systems ($\eta_{DL} \propto \rho$), originating from the contribution of the spin-momentum locking mechanism to the conversion efficiency. Liu et al. (2019) discovered crystal orientation-dependent conversion efficiency in the all-oxide heterostructure $SrTiO_3(110)/SrRuO_3/SrIrO_3$, with a damping-like torque efficiency as high as η_{DL} = 0.86 and a concomitantly substantial field-like torque efficiency. Wang et al. (2019) found that the damping-like torque efficiency of $SrTiO_3(001)/SrIrO_3$ exhibits a positive correlation with temperature by characterizing the response of the ferrimagnetic CoTb to the spin current, attaining η_{DL} = 1.2 near room temperature; additionally, they also noted that the damping-like efficiency shows no apparent dependence on the thickness of $SrIrO_3$, and the magnitude of the field-like torque efficiency is negligible. Huang et al. (2021) found a damping-like torque efficiency inversely correlated with the thickness of $SrIrO_3$ by characterizing $SrIrO_3$/LSMO grown on $SrTiO_3(001)$ substrates, which contrasts with the behaviors observed in $SrIrO_3/Py$. This correlation is attributed to be due to the additional contribution arising from the coupling of degrees of freedom at the oxide interface to the charge-spin interconversion. When the thickness of $SrIrO_3$ is several nanometers, $\eta_{DL} > 1$, but no obvious field-like torque efficiency is observed. Recently, Liu et al. (2022) observed a damping-like efficiency of η_{DL} = 0.15 at room temperature in $NdGaO_3(001)$/LSMO/$SrIrO_3$, and as the temperature decreases, the efficiency undergoes a slight increase, displaying an inverse correlation. In summary, $SrIrO_3$ showcases a remarkably significant charge-spin interconversion capability, with its damping-like efficiency surpassing 1, outperforming traditional heavy metal materials ($\eta_{DL} < 0.5$) and rivaling topological materials.

Beyond the aforementioned studies on linear charge-spin interconversion, Kozuka et al. (2021) observed a nonlinear planar Hall effect in $SrIrO_3$, as shown in Figures 4C, D. The second harmonic Hall resistance $R_{yx}^{2\omega}$ exhibits a cosine function correlation with the angle φ between the in-plane magnetic field I and the current H. Moreover, the amplitude of the second harmonic Hall resistance $\Delta R_{yx}^{2\omega}$ varies linearly with the strength of I and H. Further combining theoretical calculations, they attributed the observed nonlinear response to the contribution of the complex spin texture in the Dirac band of $SrIrO_3$ under asymmetric spin-orbit interaction. The strength, sign, and anisotropy of the nonlinear response may be linked to the spin-momentum locking properties of the complex spin texture. These findings suggest that the nonlinear planar Hall effect constitutes a novel electrical transport measurement method for probing the details of spin-momentum locking surface states and their contributions to linear/nonlinear responses. Recently, Lao et al. (2022) observed a nonlinear planar Hall effect in $SrIrO_3(110)$ thin films, similar to the findings of Kozuka et al. (2021), and discovered significant variations in the strength along different crystal orientations. Concurrently, the damping-like and field-like torque efficiencies in linear charge-spin interconversion also exhibit a high degree of crystal orientation anisotropy. Through a comprehensive analysis of the characterization results and theoretical calculations, they determined that the anisotropic charge-spin interconversion observed in $SrIrO_3(110)$ originates from contributions of both the bulk and interface. The spin Hall conductivity, which differs significantly along various crystal orientations, dominates the magnitude of the damping-like efficiency. In contrast, the variations in the strength of the nonlinear planar Hall effect and the field-like efficiency along different crystal orientations mainly arise from the contribution of anisotropic spin-momentum locking surface states, as illustrated in Figure 4E. These results indicate that combining linear and nonlinear response characterizations provides a potent approach for investigating the microscopic mechanisms of charge-spin interconversion in complex systems and their contributions to the performance of SOT devices. Collectively, the above results demonstrate that $SrIrO_3$ simultaneously harbors bulk and interface mechanisms for charge-spin interconversion, which are intimately related to the topological non-trivial characteristics in the electronic structure.

Given the high tunability of $SrIrO_3$'s topological properties under the coupling of multiple degrees of freedom, it is evident that these properties can be effectively modulated through various means, such as epitaxial strain, elemental doping, and external field stimulus. This, in turn, allows for the regulation and enhancement of the charge-spin interconversion in the system, paving the way for the realization of high-performance SOT devices. As observed in the work of Nan et al. (2019), Liu et al. (2019), Lao et al. (2022), the conversion efficiency exhibits a strong dependence on the crystal orientation, with η_{DL} = 0.5 and 0.3 for the $[1\text{-}10]_O$ and $[001]_O$ orientations of $SrIrO_3(001)$, respectively; η_{DL} = 0.9 and 0.6 for the $[\text{-}110]_{pc}$ and $[001]_{pc}$ orientations of $SrIrO_3(110)$, respectively; and η_{DL} = 0.25 and 0.46 for the $[1\text{-}10]_O$ and $[001]_O$ orientations of $SrIrO_3(110)$, respectively. Furthermore, the heterogeneous interface between $SrIrO_3$ and different magnetic materials plays a crucial role in the generation and transmission of spin current. For example, in the spin source/magnetic heterostructure grown on $SrTiO_3$ substrates, when the interface comprises $SrIrO_3$ and ferromagnetic Py, η_{DL} = 0.5 (Nan et al., 2019); when it consists of $SrIrO_3$ and ferrimagnetic CoTb, η_{DL} = 1.1 (Wang et al., 2019); and when it involves $SrIrO_3$ and the same crystal structure LSMO, η_{DL} = 1.2 (Huang et al., 2021). Concomitantly, when $SrIrO_3$ is subjected to different degrees of epitaxial strain, the conversion efficiency also undergoes significant variations. For example, the $SrIrO_3/Py$ grown on $SrTiO_3$ (Nan et al., 2019) and LSAT (Everhardt et al., 2019) substrates exhibit measured efficiencies of η_{DL} = 0.5 and 0.4, respectively; whereas the single-crystal LSMO/$SrIrO_3$ grown on $SrTiO_3$ (Liu et al., 2019) and $NdGaO_3$ (Liu et al., 2022) substrates differ in efficiency by several times, with values of approximately η_{DL} = 1.2 and 0.2, respectively. Recently, Zhang et al., (2024) achieved a significant enhancement of SOT efficiency by an order of magnitude through modulating the epitaxial strain using different substrates. By conducting ST-FMR measurements, they obtained efficiencies of 0.15, 1.05, and 1.45 for $SrIrO_3/Py$ grown on $NdGaO_3$, $SrTiO_3$, and $KTaO_3$ substrates, respectively. Based on structural measurements, the octahedral rotation patterns of $SrIrO_3$ on $NdGaO_3$, $SrTiO_3$, and $KTaO_3$ substrates were determined to be $a^0a^0c^+$, $a^-b^+c^-$, $a^-a^-c^+$, respectively, exhibiting a strong correlation with the SOT efficiency. Moreover, Cui et al. (2021) constructed a $Pb(Mg_{1/3}Nb_{2/3})_{0.7}Ti_{0.3}O_3$(PMN-PT)/$SrIrO_3$/Py heterostructure and demonstrated reversible electric field modulation based on inverse spin Hall effect via strain coupling at the epitaxial PMN-PT/$SrIrO_3$ interface using SP-FMR (Figure 4G). The above regulation methods affect the coupling strength between multiple degrees of freedom by changing the rotation of IrO_6 octahedra, thus influencing the mechanisms related to spin current generation in the electronic structure, such as the intrinsic spin Hall conductivity caused by Berry curvature, the spin-momentum locking brought by surface states, and the anisotropy that may exist at the interface due to charge transfer and orbital reconstruction. In addition to the modulation of crystal structure, adjusting the oxygen pressure constitutes a simple and widely used method. Chen et al., (2024) introduced Ir vacancies in $SrIrO_3$ by lowering the oxygen pressure during the deposition process. Although this increased the resistivity, it remarkably enhanced the spin-to-charge conversion efficiency of $SrIr_{1-x}O_3$ at room temperature, from 0.16 to 0.22 to 0.55–0.63. Due to the simultaneous increase in conversion efficiency and resistivity, the inverse spin Hall voltage in the $SrIr_{1-x}O_3$/Py heterostructure experienced a notable increase, rendering it a promising candidate for sensitive spin current detection applications. Besides, the band width and Coulomb repulsion of $SrIrO_3$ can be externally controlled via film dimension and electric gating (Gallego et al., 2023). These means provide an additional knob to manipulate the spin-orbit associated band structures, should inspire the enhancement of charge-spin conversion efficiency and interesting applications in spintronics.

In terms of spintronic applications, $SrIrO_3$ has been proven to be capable of efficiently manipulating magnetic materials and achieving deterministic switching between different magnetization states. Liu et al. (2019) used the SOT generated by $SrIrO_3$ to manipulate the magnetization state of $SrRuO_3$ with perpendicular magnetic anisotropy at 70 K, and achieved deterministic switching without an external field by fine-tuning the easy axis angle of $SrRuO_3$ through crystal structure engineering; Additionally, Liu et al. (2022) successfully switched the magnetic oxide LSMO with extremely low damping coefficient at room temperature through $SrIrO_3$. The aforementioned SOT devices based on $SrIrO_3$ only require a threshold current of 3-5 × 10^6 A/cm^2, which demonstrates lower energy consumption compared to traditional heavy metal spin source materials. Moreover, Ren et al. (2022) constructed a heterostructure comprising $SrIrO_3$ and a ferrimagnetic insulating oxide with perpendicular magnetic anisotropy, and observed spin Hall magnetoresistance and spin Hall anomalous magnetoresistance, opening up the possibility for realizing all-oxide insulating spintronics. Recently, Tang et al. (2022) designed an $SrIrO_3$/FeGd heterostructure and achieved room-temperature SOT-driven magnetization switching with a low threshold current density of 3×10^6 A/cm^2 under the application of a small in-plane magnetic field (Figure 4H), highlighting the crucial role of $SrIrO_3$ in the development of energy-efficient spintronic devices. Simultaneously, combining $SrIrO_3$ with magnetic oxides in an all-oxide system can meet the material requirements of spintronic devices such as spin storage, transmission, logic, and magnetic oscillators, rendering it an ideal platform for realizing multifunctional spintronic devices. Furthermore, Everhardt et al. (2019) also performed SOT characterization in the layered perovskite structure Sr_2IrO_4, reporting an efficiency of around 0.1. Additional research on SOT regulation, magnetic moment switching, and other $Sr_{n+1}Ir_nO_{3n+1}$ compounds with RP structure is imperative.

The above results confirm that $SrIrO_3$ exhibits highly efficient and tunable charge-spin interconversion, holding promise for the realization of multifunctional spintronic devices. However, there are still some deficiencies in understanding the contribution of each mechanism to the charge-spin conversion efficiency. Firstly, it is currently widely believed that the damping-like efficiency of $SrIrO_3$ originates from the spin Hall conductivity. However, based on the measurement results of $SrIrO_3$/LSMO (Huang et al., 2021) and other topological materials (Mellnik et al., 2014; Li et al., 2018), as well as theoretical calculations (Amin and Stiles, 2016), spin-momentum locking also contributes to the damping-like efficiency, necessitating the clarification of the specific physical mechanisms. Secondly, although spin-momentum locking can contribute to the field-like efficiency, there is a large discrepancy in the actual η_{FL} values observed in $SrIrO_3$. For example, in $SrIrO_3$/(Py, LSMO, CoTb), η_{FL} < 0.1, while in $SrIrO_3$/$SrRuO_3$, η_{FL} > 1. This suggests that in addition to spin-momentum locking, there may be influences from proximity effects, spin transparency, ferromagnetism/ferrimagnetism, etc., at the actual interface, which need to be systematically investigated and explored in future studies to gain a comprehensive understanding of the charge-spin conversion mechanisms in $SrIrO_3$-based systems.

3.3.2 Potassium tantalate

Potassium tantalate ($KTaO_3$) is a perovskite-structured insulating material with tantalum ions in its oxygen octahedra exhibiting a $5d^0$ orbital arrangement. As a result, many of its basic properties are similar to those of $SrTiO_3$, including a wide bandgap (Nakamura and Kimura, 2009), the presence of a 2DEG at the surface/interface (King et al., 2012; Santander-Syro et al., 2012; Bruno et al., 2019), and associated superconductivity (Chen et al., 2021; Liu et al., 2021). However, $KTaO_3$ distinguish itself from $SrTiO_3$ by its stronger SOC, which causes further splitting of the triply degenerate t_{2g} orbitals, leading to more intricate electronic structures. King et al. (2012) and Santander-Syro et al. (2012). investigated the electronic structure of the $KTaO_3$ (001) surface by using ARPES, confirming the existence of multiple sub-band crossings near the Fermi level. Unlike the insulating nature of the bulk, these observed electron bands demonstrate good conductivity at the $KTaO_3$ surface, indicative of a 2DEG state. Furthermore, the carriers in these bands exhibit varying effective masses, a consequence of the interplay between SOC and correlation effects of comparable strength, and quantum confinement. Despite these findings, King et al. (2012) and Santander-Syro et al. (2012). were unable to directly observe the Rashba-split bands in the 2DEG. Recently, Varotto et al. (2022) successfully observed the Rashba-split bands of the 2DEG in $KTaO_3$(001)/Al using ARPES. By fitting these bands, they identified band pairs arising from different orbital combinations. As illustrated in Figure 5A, the pink and green band pairs are primarily composed of d_{xy} orbitals, while the orange band pair consists of mixed d_{xz} and d_{yz} orbitals and exhibits pronounced Rashba splitting. The cyan band, on the other hand, is attributed to additional d_{xy} sub-bands originating from quantum confinement effects. This direct observation of Rashba-split bands in $KTaO_3$-2DEG offers deeper insights into the complex multi-orbital nature of the band structure. The spatial inversion asymmetry at

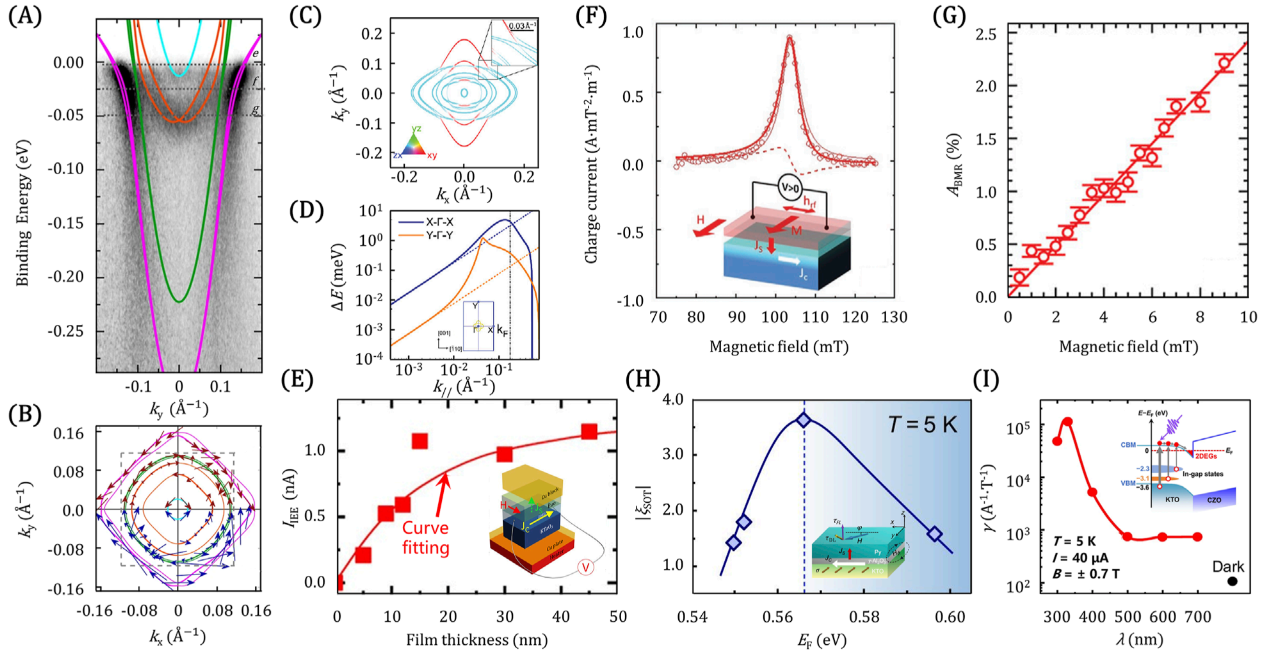

FIGURE 5
Electronic structures, spin transport properties and SOT-related characterization results of $KTaO_3$: **(A)** ARPES results of surface 2DEG in $KTaO_3$(001). The measured band structure is represented by colored lines: pink and green correspond to d_{xy} orbitals, orange corresponds to mixed d_{xz} and d_{yz} orbitals, and cyan corresponds to additional d_{xy} sub-bands arising from quantum confinement effects (Reproduced with permission from Ref (Varotto et al., 2022).); **(B)** Spin and orbital textures of the spin-momentum locked Fermi surface states. The upper quadrant shows the spin texture (red arrows), while the lower quadrant shows the orbital texture (blue arrows) (Reproduced with permission from Ref (Varotto et al., 2022).); **(C)** Anisotropic orbital-projected Fermi surface in $KTaO_3$(110)-2DEG (Reproduced with permission from Ref (Martínez et al., 2023).) **(D)** Energy difference (ΔE) between the up and down spin states along the high-symmetry paths $X-\Gamma-X$ (blue) and $Y-\Gamma-Y$ (orange) The inset shows the first Brillouin zone and crystal orientation (Adapted with permission from Ref (Martínez et al., 2023).); **(E)** Correlation between the measured inverse Edelstein current and EuO thickness. The inset illustrates thermal spin injection and inverse Edelstein effect at the $KTaO_3$/EuO interface (Adapted with permission from Ref (Zhang et al., 2019b).); **(F)** Dependence of the charge current generated through the inverse Rashba-Edelstein effect on the applied magnetic field. The inset shows the configuration of the SP-FMR measurement (Reproduced with permission from Ref (Vicente-Arche et al., 2021); **(G)** Relationship between the bilinear magnetoresistance and the magnetic field (Reproduced with permission from Ref (Vicente-Arche et al., 2021); **(H)** Variation of the charge-spin conversion efficiency with the Fermi energy at 5K. The dashed line indicates the Lifshitz transition. The inset shows a schematic of the $KTaO_3$(001)/γ-Al_2O_3/Py device structure and the ST-FMR experimental setup (Adapted with permission from Ref (Zhang et al., 2023).); **(I)** Nonreciprocal transport coefficient as a function of light wavelength under illumination (Adapted with permission from Ref (Zhang et al., 2024)).

the surface/interface induces spin splitting in the 2DEG under the Rashba effect, resulting in the formation of spin-momentum locked surface state (Figure 5B). The orange band pair, in particular, displays a substantial band splitting. Theoretical calculations yield an effective Rashba parameter α_R of approximately 320 meV · Å, which is consistent with magneto-transport measurements ($\alpha_R \approx 300$ meV · Å) (Vicente-Arche et al., 2021) and conducive to efficient charge-spin conversion. Although the spin and orbital textures deviate somewhat from the pure linear Rashba model, they generally adhere to the characteristics of the Rashba effect.

Beyond the (001) orientation, Bruno et al. (2019) also observed similar electronic structure characteristics of 2DEG in $KTaO_3$(111). However, due to the contribution of all t_{2g} orbitals and the (111) crystal symmetry, a distinctive star-shaped-hexagonal Fermi surface emerges. This unique symmetry gives rise to novel spin-momentum locking properties: unlike the classical Rashba picture, the momentum splitting on the star-shaped-hexagonal Fermi surface is non-constant, and spin-momentum locking is only present along high-symmetry directions, accompanied by an out-of-plane spin component. These characteristics play a crucial role in generating special spin polarizations for charge-spin interconversion. Martínez et al. (2023) investigated the electronic structure of the 2DEG formed by depositing a thin Al layer on the $KTaO_3$(110) surface using ARPES, revealing significantly anisotropic orbital characteristics. The Fermi surface consists of two elliptical contours with mutually perpendicular major axes (Figure 5C). The long axis along the [001] direction corresponds to d_{xy} orbital characteristics, while the [−110] direction is associated with d_{zx}/d_{yz} orbital characteristics. By fitting the band results, they discovered an unconventional and anisotropic Rashba splitting, with the Rashba splitting value along the $\Gamma-X$ direction ([−110] direction) being significantly larger than that along the $\Gamma-Y$ direction ([001] direction), differing by approximately an order of magnitude (Figure 5D). This anisotropic Rashba effect is attributed to the enhanced interaction between orbital and spin angular momentum, offering new insights for interpreting spin-orbit electronic correlation experiments. In addition to the aforementioned studies, heterostructures of $KTaO_3$ with $LaTiO_3$ (Zou et al., 2015), $LaAlO_3$ (Zhang et al., 2017; Zhang et al., 2019a), EuO (Zhang et al., 2018), $LaVO_3$ (Wadehra et al., 2020) have also been found to host 2DEGs, exhibiting novel properties including high mobility of interface carriers, spin polarization, and high tunability of spin-related parameters.

The strong spin-orbit coupling and unique electronic band structure of the $KTaO_3$ interface 2DEG have sparked significant interest in exploring its charge-spin interconversion properties. Zhang et al. (2019b) successfully generated a 1 nA charge current through the inverse Edelstein effect by employing thermal spin injection in the $KTaO_3$/EuO interface 2DEG system (Figure 5E). The use of thermal spin injection, which is driven by a temperature gradient, effectively eliminates potential parasitic effects associated with ferromagnetic resonance. Furthermore, by characterizing the spin Seebeck coefficient of the system, they qualitatively confirmed that the $KTaO_3$/EuO system exhibits a charge-spin conversion efficiency significantly higher than that of the conversional Pt/YIG system. In a recent study, Vicente-Arche et al. (2021) quantitatively characterized the charge-spin conversion efficiency of the $KTaO_3$/Al interface by two methods: SP-FMR and unidirectional magnetoresistance (UMR). In the SP-FMR experiment, they injected spin current into the 2DEG using an adjacent Py layer and obtained a conversion efficiency of λ_{IEE} ~ - 3.5 nm for the two-dimensional system by measuring the transverse charge current generated by the inverse Rashba-Edelstein effect (Figure 5F). Concurrently, they observed the bilinear magnetoresistance effect related to charge-spin interconversion arising from the Rashba-Edelstein effect in the 2DEG by characterizing the UMR (Figure 5G). Further calculations yielded λ_{IEE} ~ - 6–25 nm. Although the complex multi-band contribution of the 2DEG introduces some deviations in the estimation of the results, these two characterization methods provide compelling evidence that $KTaO_3$ possesses a substantial conversion efficiency comparable to that of the $SrTiO_3$ system (Table 1). Moreover, Zhang et al. (2023) pioneered the use of spin torque-ferromagnetic resonance (ST-FMR) measurements to achieve charge-spin interconversion in $KTaO_3$-based systems. They quantitatively determined the charge-spin conversion induced by spin-momentum locking at the $KTaO_3(001)/\gamma\text{-}Al_2O_3$ interface. Remarkably, the conversion efficiency of the $KTaO_3(001)/\gamma\text{-}Al_2O_3$/Py devices reached values as high as 3.6 and 1.1 at 5 K and 300 K, respectively, surpassing the conversion efficiency of Pt by more than an order of magnitude. The $KTaO_3(001)/\gamma\text{-}Al_2O_3$ interface demonstrates an even more impressive conversion efficiency compared to the $KTaO_3$/EuO interface, suggesting that the charge-spin interconversion properties of the $KTaO_3$ 2DEG can be tuned and enhanced through the selection of different heterointerfaces.

The significant SOC and complex carrier transport properties at the interface of $KTaO_3$ make its electronic structure and charge-spin interconversion properties more sensitive and tunable. Zhang et al. (2023) not only obtained a large charge-spin conversion efficiency at the $KTaO_3(001)/\gamma\text{-}Al_2O_3$ interface but also observed a strong dependence of the conversion efficiency on the band filling state at low temperatures (5 K) (Figure 5H). They controlled the Fermi level filling state by adjusting the thickness of $\gamma\text{-}Al_2O_3$. At low Fermi energies, only one type of carrier exists in the 2DEG, occupying the lower energy d_{xy} band. When the Fermi energy increases to around 0.566 eV, the carriers in the 2DEG change from one type to two types, undergoing a Lifshitz transition and reaching a maximum conversion efficiency of 3.6. This is due to the Fermi level rising to the bottom of the d_{zx}/d_{yz} band, causing orbital mixing and enhanced Rashba splitting. As the Fermi energy further increases, the Rashba splitting of the d_{zx}/d_{yz} band decreases, and the conversion efficiency rapidly drops to 1.6. In addition, the regulation of the Fermi level filling state by light illumination is also significant. Gan et al. (2023) conducted light illumination experiments with different wavelengths and intensities on the superconducting $KTaO_3(110)/Hf_{0.5}Zr_{0.5}O_2$ heterojunction. By observing the weak anti-localization (WAL) effect through magnetic field-dependent resistance measurements, they found that the Rashba spin-orbit coupling (RSOC) strength increased by 7 times under light illumination, i.e., the RSOC-induced effective magnetic field B_{so} increased from 1.9 T to 12.6 T. This is because under laser irradiation, electrons are excited from the gap states to the Ta 5d t_{2g} conduction band, increasing the carrier density of the system. This leads to a rise in the Fermi level, crossing more Ta-t_{2g} conduction bands and significantly enhancing the RSOC effect. Recently, Zhang et al. (2024b) also controlled the nonreciprocal transport in the $KTaO_3$ system by light illumination. They analyzed the bilinear characteristics of magnetoresistance under light illumination (i.e., $\Delta R/R_0$ is linearly related to current density and magnetic field) and observed a three-order-of-magnitude enhancement of the nonreciprocal transport coefficient in the superconducting $KTaO_3(111)/CaZrO_3$ heterojunction, reaching 10^5 A^{-1} T^{-1} (Figure 5I). This is due to the pumping of a large number of electrons from the valence band to the Ta-t_{2g} conduction band of $KTaO_3$ under light illumination, resulting in a larger RSOC strength and additional high-mobility photocarriers. This study promotes the potential application of $KTaO_3$ in photorectification devices and spin-orbit devices.

Although the current research on the charge-spin interconversion of $KTaO_3$ is still in its infancy, its excellent performance comparable to $SrTiO_3$, indicates its enormous potential as a spin source material. Moreover, its rich and tunable electronic structure and charge-spin interconversion properties suggest that $KTaO_3$ is an outstanding material for exploring novel quantum states and related new spintronic devices.

4 Outlook

Compared to the heavy metal systems, which have been extensively studied as spin source materials in early SOT devices, transition metal oxides have rapidly gained significant attention in this field. The 3d-5d perovskite family, including $SrTiO_3$, $SrRuO_3$, $SrIrO_3$, and $KTaO_3$, are typical representatives of this material system, showing excellent performance in terms of both charge-spin conversion efficiency and switching threshold current (Table 1). These materials exhibit several advantages, such as rich physical properties, versatile control over multiple degrees of freedom, and excellent crystal structure compatibility. By leveraging these advantages, transition metal oxides emerge as an ideal material platform for designing and realizing novel spintronic devices.

Since recent research has focused on only a few materials, there are still many systems with great potential in the vast transition metal oxide family that await further exploration. By designing oxide heterostructures and exploiting the ability of interfaces to control crystal structure, magnetoelectric properties, and electronic structure, researchers expect to significantly influence and enhance charge-spin interconversion (Ramesh and Schlom, 2019; Hwang et al., 2012). This can be achieved, for example, by inducing spin transport properties that cannot be present in a single bulk phase through the use of multi-component superlattices, or by maintaining high conversion efficiency up to room temperature in 2DEG systems via interface design. Moreover, by engineering the symmetry of complex oxide systems, the spin orientation of the generated spin current can be effectively manipulated, enabling achieve all-electric switching of the magnetization state, which is a crucial step toward practical applications. In heavy metals and two-dimensional materials, constructing symmetry-broken structures, such as creating vertical or lateral material composition gradients, incorporating antiferromagnets, or using ferroelectric materials (Yu et al., 2014; Oh et al., 2016; Zheng et al., 2021), can generate spin currents with out-of-plane spin polarization. This allows for deterministic switching of perpendicular moments without the need of an external magnetic field, which is essential for the realization of low-power, high-density SOT devices. In transition metal oxides, the spin-momentum locking in the surface state of $SrTiO_3$(111) 2DEG has an out-of-plane spin polarization component (He et al., 2018a), making it promising system for realizing deterministic switching of perpendicular moments without an external field. Although there are no relevant reports in other oxides yet, it is feasible to influence the symmetry by fine-tuning the material composition and crystal structure during the growth process, and related research should also be carried out systematically in the future. Furthermore, substituting the *B*-site atomic species in ABO_3-type perovskite oxides with elements such as Rh, Mo, as in $SrRhO_3$ and $SrMoO_3$, may lead to richer electronic structures and SOT properties. The investigation of SOT in layered perovskite structures, such as Sr_2IrO_4, is also relatively preliminary, and the SOT properties and their manipulation in various layered perovskite materials warrant further exploration. Additionally, other structured oxides have shown the potential for excellent charge-spin interconversion properties. For example, a sizeable Rashba splitting has been observed in the delafossite structure $PdCoO_2$ (Lee et al., 2021), and a new type of spin torque generated by anisotropic spin splitting has been observed in the rutile structure RuO_2 (González-Hernández et al., 2021; Bai et al., 2022; Bose et al., 2022). The spin-charge interconversion in oxide thin films and heterostructures with spinel, pyroxene, double perovskite, and other structure remains to be investigated.

In addition to expanding the range of materials, researchers anticipate achieving precise control over SOT strength in transition metal oxide thin films and heterostructures by leveraging the characteristics of multi degrees of freedom coupling. The aforementioned spin Hall effect and surface states contribute differently to the damping-like torque and field-like torque of spin-orbit torque, and the ratio of these two components can significantly affect the energy consumption and response time of the magnetization switching process, domain wall motion velocity, and other dynamic processes (Katine et al., 2000; Legrand et al., 2015; Yoon et al., 2017; Liu et al., 2021; Taniguchi et al., 2015; Gomonay et al., 2016; Zhu and Zhao, 2020). Therefore, by influencing the electronic structure through multiple degrees of freedom, precise control of the strength and direction of the damping-like torque and field-like torque, respectively, is an important research direction for realizing high-performance SOT devices.

Finally, establishing the correlation between the electronic structure of oxides and charge-spin interconversion is crucial for understanding and controlling device performance. Currently, in the 2DEG of the 3*d* oxide $SrTiO_3$, the relatively simple band structure can be well linked with the charge-spin interconversion, and the contribution of the novel electronic structure found to the conversion efficiency can be well interpreted by theory. However, for 4*d* and 5*d* oxides with strong SOC, it is essential to combine first-principles calculations with experimental techniques such as ARPES to determine their complex electronic band structures. This will enable researchers to establish the correlation rules between the electronic band structure and spin transport properties, and to gain a profound understanding of the origin of the significant charge-spin interconversion in these systems, ultimately enhancing the charge-spin conversion efficiency. One approach is to systematically correlate the electronic structure, crystal structure, and charge-spin conversion efficiency by continuously tuning of a single variable, such as chemical doping of the same group elements. Furthermore, as mentioned above, the influence of the electronic structure to the charge-spin interconversion is not only reflected in the SOT under linear response but also in the novel spin transport phenomena that emerge under nonlinear response (He et al., 2018a; He et al., 2018b; Lao et al., 2022; Kozuka et al., 2021; Lee et al., 2021;Yasuda et al., 2017; Dyrdał et al., 2020; Kumar et al., 2021; Rao et al., 2021; Yu et al., 2021). For example, the nonlinear planar Hall effect observed in oxides $PdCoO_2$ (Lee et al., 2021) and $SrIrO_3$ (Lao et al., 2022; Kozuka et al., 2021) well confirms the existence of surface states caused by non-trivial band structures in their electronic structures. In addition, Lao et al. (2022) further explored the contribution of spin Hall effect and surface states to the charge-spin conversion efficiency by combining the characterization of linear and nonlinear responses and discussing the correlation between SOT and nonlinear planar Hall effect. Combining linear and nonlinear response characterization methods can decouple the contributions brought by different mechanisms and will become a powerful tool for clarifying the role of electronic structure in charge-spin interconversion.

Author contributions

YH: Writing–review and editing, Writing–original draft. BL: Writing–review and editing. XZ: Writing–review and editing. SL: Writing–review and editing. R-WL: Writing–review and editing. ZW: Writing–review and editing, Writing–original draft, Funding acquisition.

Funding

The author(s) declare that financial support was received for the research, authorship, and/or publication of this article. This work was supported by the National Key Research and Development Program of China (Nos 2019YFA0307800 and 2017YFA0303600), the National Natural Science Foundation of China (Nos 12174406, 11874367, 51931011, and 52127803), the Ningbo Key Scientific and

Technological Project (Grant No. 2022Z094), the Ningbo Natural Science Foundation (No. 2023J411).

Conflict of interest

The authors declare that the research was conducted in the absence of any commercial or financial relationships that could be construed as a potential conflict of interest.

Publisher's note

All claims expressed in this article are solely those of the authors and do not necessarily represent those of their affiliated organizations, or those of the publisher, the editors and the reviewers. Any product that may be evaluated in this article, or claim that may be made by its manufacturer, is not guaranteed or endorsed by the publisher.

References

Agarwal, S., Aimone, B., Akinaga, H., Akinola, O., Badaroglu, M., Bersuker, G., et al. (2021). Beyond CMOS 2018. *Int. Roadmap For Devices And Syst.*, 1–129. doi:10.1109/IRDS54852.2021.00011

Amin, V. P., and Stiles, M. D. (2016). Spin transport at interfaces with spin-orbit coupling: phenomenology. *Phys. Rev. B* 94 (10), 104420. doi:10.1103/PhysRevB.94.104420

Armitage, N. P., Mele, E. J., and Vishwanath, A. (2018). Weyl and Dirac semimetals in three-dimensional solids. *Rev. Mod. Phys.* 90 (1), 015001. doi:10.1103/RevModPhys.90.015001

Bai, H., Han, L., Feng, X. Y., Zhou, Y., Su, R., Wang, Q., et al. (2022). Observation of spin splitting torque in a collinear antiferromagnet RuO_2. *Phys. Rev. Lett.* 128 (19), 197202. doi:10.1103/PhysRevLett.128.197202

Ben Shalom, M., Sachs, M., Rakhmilevitch, D., Palevski, A., and Dagan, Y. (2010). Tuning spin-orbit coupling and superconductivity at the $SrTiO_3/LaAlO_3$ interface: a magnetotransport study. *Phys. Rev. Lett.* 104 (12), 126802. doi:10.1103/PhysRevLett.104.126802

Berger, L. (1996). Emission of spin waves by a magnetic multilayer traversed by a current. *Phys. Rev. B* 54 (13), 9353–9358. doi:10.1103/PhysRevB.54.9353

Bose, A., Schreiber, N. J., Jain, R., Shao, D. F., Nair, H. P., Sun, J., et al. (2022). Tilted spin current generated by the collinear antiferromagnet ruthenium dioxide. *Nat. Electron.* 5 (5), 267–274. doi:10.1038/s41928-022-00744-8

Bruno, F. Y., McKeown Walker, S., Riccò, S., de la Torre, A., Wang, Z., Tamai, A., et al. (2019). Band structure and spin–orbital texture of the (111)-$KTaO_3$ 2D electron gas. *Adv. Electron. Mater.* 5 (5). doi:10.1002/aelm.201800860

Carter, J.-M., Shankar, V. V., Zeb, M. A., and Kee, H. Y. (2012). Semimetal and topological insulator in perovskite iridates. *Phys. Rev. B* 85 (11), 115105. doi:10.1103/PhysRevB.85.115105

Caviglia, A. D., Gabay, M., Gariglio, S., Reyren, N., Cancellieri, C., and Triscone, J. M. (2010). Tunable Rashba spin-orbit interaction at oxide interfaces. *Phys. Rev. Lett.* 104 (12), 126803. doi:10.1103/PhysRevLett.104.126803

Chai, Y., Liang, Y., Xiao, C., Wang, Y., Li, B., Jiang, D., et al. (2023). Multiferroic magnon spin-torque based reconfigurable logic-in-memory. *arXiv Prepr. arXiv:2309.14614*.

Chen, H., Jiang, D., Zhang, Q., Liang, Y., Liu, J., Tang, A., et al. (2024). Tuning stoichiometry for enhanced spin-charge interconversion in transition metal oxides. *Adv. Electron. Mater.* 10 (4), 2300666. doi:10.1002/aelm.202300666

Chen, H., and Yi, D. (2021). Spin–charge conversion in transition metal oxides. *Apl. Mater.* 9 (6). doi:10.1063/5.0052304

Chen, Y., Bergman, D. L., and Burkov, A. A. (2013). Weyl fermions and the anomalous Hall effect in metallic ferromagnets. *Phys. Rev. B* 88 (12), 125110. doi:10.1103/PhysRevB.88.125110

Chen, Y., Lu, Y.-M., and Kee, H.-Y. (2015). Topological crystalline metal in orthorhombic perovskite iridates. *Nat. Commun.* 6 (1), 6593. doi:10.1038/ncomms7593

Chen, Z., Liu, Y., Zhang, H., Liu, Z., Tian, H., Sun, Y., et al. (2021). Electric field control of superconductivity at the $LaAlO_3/KTaO_3(111)$ interface. *Science* 372 (6543), 721–724. doi:10.1126/science.abb3848

Cui, D., Xu, Y., Zhou, L., Zhang, L., Luan, Z., Li, C., et al. (2021). Electrically tunable inverse spin Hall effect in $SrIrO_3/Pb(Mg_{1/3}Nb_{2/3})_{0.7}$ $Ti_{0.3}O_3$ heterostructures through interface strain coupling. *Appl. Phys. Lett.* 118 (5), 052904. doi:10.1063/5.0027125

Dieny, B., Prejbeanu, I. L., Garello, K., Gambardella, P., Freitas, P., Lehndorff, R., et al. (2020). Opportunities and challenges for spintronics in the microelectronics industry. *Nat. Electron.* 3 (8), 446–459. doi:10.1038/s41928-020-0461-5

Dyrdał, A., Barnaś, J., and Fert, A. (2020). Spin-momentum-locking inhomogeneities as a source of bilinear magnetoresistance in topological insulators. *Phys. Rev. Lett.* 124 (4), 046802. doi:10.1103/PhysRevLett.124.046802

Everhardt, A. S., Dc, M., Huang, X., Sayed, S., Gosavi, T. A., Tang, Y., et al. (2019). Tunable charge to spin conversion in strontium iridate thin films. *Phys. Rev. Mater.* 3 (5), 051201. doi:10.1103/PhysRevMaterials.3.051201

Fang, Z., Nagaosa, N., Takahashi, K. S., Asamitsu, A., Mathieu, R., Ogasawara, T., et al. (2003). The anomalous Hall effect and magnetic monopoles in momentum space. *Science* 302 (5642), 92–95. doi:10.1126/science.1089408

Fujioka, J., Yamada, R., Kawamura, M., Sakai, S., Hirayama, M., Arita, R., et al. (2019). Strong-correlation induced high-mobility electrons in Dirac semimetal of perovskite oxide. *Nat. Commun.* 10 (1), 362. doi:10.1038/s41467-018-08149-y

Gallego, F., Tornos, J., Beltran, J. I., Peralta, A., Garcia-Barriocanal, J., Yu, G., et al. (2023). Reversible metal-insulator transition in $SrIrO_3$ ultrathin layers by field effect control of inversion symmetry breaking. *Commun. Mater.* 4 (1), 36. doi:10.1038/s43246-023-00362-7

Gallego, F., Trier, F., Mallik, S., Bréhin, J., Varotto, S., Moreno Vicente-Arche, L., et al. (2024). All-electrical detection of the spin-charge conversion in nanodevices based on $SrTiO_3$ 2-D electron gases. *Adv. Funct. Mater.* 34 (3), 2307474. doi:10.1002/adfm.202307474

Gan, Y., Yang, F., Kong, L., Chen, X., Xu, H., Zhao, J., et al. (2023). Light-induced giant Rashba spin–orbit coupling at superconducting $KTaO_3(110)$ heterointerfaces. *Adv. Mater.* 35 (25), 2300582. doi:10.1002/adma.202300582

Gomonay, O., Jungwirth, T., and Sinova, J. (2016). High antiferromagnetic domain wall velocity induced by néel spin-orbit torques. *Phys. Rev. Lett.* 117 (1), 017202. doi:10.1103/PhysRevLett.117.017202

González-Hernández, R., Šmejkal, L., Výborný, K., Yahagi, Y., Sinova, J., Jungwirth, T., et al. (2021). Efficient electrical spin splitter based on nonrelativistic collinear antiferromagnetism. *Phys. Rev. Lett.* 126 (12), 127701. doi:10.1103/PhysRevLett.126.127701

Grezes, C., Kandazoglou, A., Cosset-Cheneau, M., Arche, L. M. V., Noël, P., Sgarro, P., et al. (2023). Non-volatile electric control of spin-orbit torques in an oxide two-dimensional electron gas. *Nat. Commun.* 14 (1), 2590. doi:10.1038/s41467-023-37866-2

Grigera, S. A., Gegenwart, P., Borzi, R. A., Weickert, F., Schofield, A. J., Perry, R. S., et al. (2004). Disorder-sensitive phase formation linked to metamagnetic quantum criticality. *Science* 306 (5699), 1154–1157. doi:10.1126/science.1104306

Haidar, S. M., Shiomi, Y., Lustikova, J., and Saitoh, E. (2015). Enhanced inverse spin Hall contribution at high microwave power levels in $La_{0.67}Sr_{0.33}MnO_3/SrRuO_3$ epitaxial bilayers. *Appl. Phys. Lett.* 107 (15). doi:10.1063/1.4933379

He, P., Walker, S. M., Zhang, S. S. L., Bruno, F., Bahramy, M., Lee, J. M., et al. (2018a). Observation of out-of-plane spin texture in a $SrTiO_3(111)$ two-dimensional electron gas. *Phys. Rev. Lett.* 120 (26), 266802. doi:10.1103/PhysRevLett.120.266802

He, P., Zhang, S. S. L., Zhu, D., Liu, Y., Wang, Y., Yu, J., et al. (2018b). Bilinear magnetoelectric resistance as a probe of three-dimensional spin texture in topological surface states. *Nat. Phys.* 14 (5), 495–499. doi:10.1038/s41567-017-0039-y

He, P., Zhang, S. S. L., Zhu, D., Shi, S., Heinonen, O. G., Vignale, G., et al. (2019). Nonlinear planar Hall effect. *Phys. Rev. Lett.* 123 (1), 016801. doi:10.1103/PhysRevLett.123.016801

Huang, X., Sayed, S., Mittelstaedt, J., Susarla, S., Karimeddiny, S., Caretta, L., et al. (2021). Novel spin–orbit torque generation at room temperature in an all-oxide epitaxial $La_{0.7}Sr_{0.3}MnO_3/SrIrO_3$ system. *Adv. Mater.* 33 (24), e2008269. doi:10.1002/adma.202008269

Hwang, H. Y., Iwasa, Y., Kawasaki, M., Keimer, B., Nagaosa, N., and Tokura, Y. (2012). Emergent phenomena at oxide interfaces. *Nat. Mater.* 11 (2), 103–113. doi:10.1038/nmat3223

Imada, M., Fujimori, A., and Tokura, Y. (1998). Metal-insulator transitions. *Rev. Mod. Phys.* 70 (4), 1039–1263. doi:10.1103/RevModPhys.70.1039

Itoh, S., Endoh, Y., Yokoo, T., Ibuka, S., Park, J. G., Kaneko, Y., et al. (2016). Weyl fermions and spin dynamics of metallic ferromagnet $SrRuO_3$. *Nat. Commun.* 7 (1), 11788. doi:10.1038/ncomms11788

Jadaun, P., Register, L. F., and Banerjee, S. K. (2020). Rational design principles for giant spin Hall effect in 5*d* -transition metal oxides. *Proc. Natl. Acad. Sci.* 117 (22), 11878–11886. doi:10.1073/pnas.1922556117

Jin, M.-J., Moon, S. Y., Park, J., Modepalli, V., Jo, J., Kim, S. I., et al. (2017). Nonlocal spin diffusion driven by giant spin Hall effect at oxide heterointerfaces. *Nano Lett.* 17 (1), 36–43. doi:10.1021/acs.nanolett.6b03050

Kaneta-Takada, S., Kitamura, M., Arai, S., Arai, T., Okano, R., Anh, L. D., et al. (2022). Giant spin-to-charge conversion at an all-epitaxial single-crystal-oxide Rashba interface with a strongly correlated metal interlayer. *Nat. Commun.* 13 (1), 5631. doi:10.1038/s41467-022-33350-5

Katine, J. A., Albert, F. J., Buhrman, R. A., Myers, E. B., and Ralph, D. C. (2000). Current-driven magnetization reversal and spin-wave excitations in Co/Cu/Co pillars. *Phys. Rev. Lett.* 84 (14), 3149–3152. doi:10.1103/PhysRevLett.84.3149

Kim, B. J., Jin, H., Moon, S. J., Kim, J.-Y., Park, B. G., Leem, C. S., et al. (2008). Novel $_{\mathrm{eff}}$=1/2 Mott state induced by relativistic spin-orbit coupling in Sr_2IrO_4. *Phys. Rev. Lett.* 101 (7), 076402. doi:10.1103/PhysRevLett.101.076402

Kim, H.-S., Chen, Y., and Kee, H.-Y. (2015). Surface states of perovskite iridates $AIrO_3$: signatures of a topological crystalline metal with nontrivial Z_2 index. *Phys. Rev. B* 91 (23), 235103. doi:10.1103/PhysRevB.91.235103

King, P. D. C., He, R. H., Eknapakul, T., Buaphet, P., Mo, S. K., Kaneko, Y., et al. (2012). Subband structure of a two-dimensional electron gas formed at the polar surface of the strong spin-orbit perovskite $KTaO_3$. *Phys. Rev. Lett.* 108 (11), 117602. doi:10.1103/PhysRevLett.108.117602

King, P. D. C., McKeown Walker, S., Tamai, A., de la Torre, A., Eknapakul, T., Buaphet, P., et al. (2014). Quasiparticle dynamics and spin–orbital texture of the $SrTiO_3$ two-dimensional electron gas. *Nat. Commun.* 5 (1), 3414. doi:10.1038/ncomms4414

Koster, G., Klein, L., Siemons, W., Rijnders, G., Dodge, J. S., Eom, C. B., et al. (2012). Structure, physical properties, and applications of $SrRuO_3$ thin films. *Rev. Mod. Phys.* 84 (1), 253–298. doi:10.1103/RevModPhys.84.253

Kozuka, Y., Isogami, S., Masuda, K., Miura, Y., Das, S., Fujioka, J., et al. (2021). Observation of nonlinear spin-charge conversion in the thin film of nominally centrosymmetric Dirac semimetal $SrIrO_3$ at room temperature. *Phys. Rev. Lett.* 126 (23), 236801. doi:10.1103/PhysRevLett.126.236801

Kumar, D., Hsu, C.-H., Sharma, R., Chang, T. R., Yu, P., Wang, J., et al. (2021). Room-temperature nonlinear Hall effect and wireless radiofrequency rectification in Weyl semimetal $TaIrTe_4$. *Nat. Nanotechnol.* 16 (4), 421–425. doi:10.1038/s41565-020-00839-3

Lao, B., Liu, P., Zheng, X., Lu, Z., Li, S., Zhao, K., et al. (2022). Anisotropic linear and nonlinear charge-spin conversion in topological semimetal $SrIrO_3$. *Phys. Rev. B* 106 (22), L220409. doi:10.1103/PhysRevB.106.L220409

Lee, J. H., Harada, T., Trier, F., Marcano, L., Godel, F., Valencia, S., et al. (2021). Nonreciprocal transport in a Rashba ferromagnet, delafossite $PdCoO_2$. *Nano Lett.* 21 (20), 8687–8692. doi:10.1021/acs.nanolett.1c02756

Legrand, W., Ramaswamy, R., Mishra, R., and Yang, H. (2015). Coherent subnanosecond switching of perpendicular magnetization by the fieldlike spin-orbit torque without an external magnetic field. *Phys. Rev. Appl.* 3 (6), 064012. doi:10.1103/PhysRevApplied.3.064012

Lesne, E., Fu, Y., Oyarzun, S., Rojas-Sánchez, J. C., Vaz, D. C., Naganuma, H., et al. (2016). Highly efficient and tunable spin-to-charge conversion through Rashba coupling at oxide interfaces. *Nat. Mater.* 15 (12), 1261–1266. doi:10.1038/nmat4726

Li, J., Wang, J., Wuttig, M., Ramesh, R., Wang, N., Ruette, B., et al. (2004). Dramatically enhanced polarization in (001), (101), and (111) $BiFeO_3$ thin films due to epitiaxial-induced transitions. *Appl. Phys. Lett.* 84 (25), 5261–5263. doi:10.1063/1.1764944

Li, P., Wu, W., Wen, Y., Zhang, C., Zhang, J., Zhang, S., et al. (2018). Spin-momentum locking and spin-orbit torques in magnetic nano-heterojunctions composed of Weyl semimetal WTe_2. *Nat. Commun.* 9 (1), 3990. doi:10.1038/s41467-018-06518-1

Li, S., Lao, B., Lu, Z., Zheng, X., Zhao, K., Gong, L., et al. (2023). Room temperature spin-orbit torque efficiency and magnetization switching in $SrRuO_3$-based heterostructures. *Phys. Rev. Mater.* 7 (2), 024418. doi:10.1103/PhysRevMaterials.7.024418

Lin, W., Liu, L., Liu, Q., Li, L., Shu, X., Li, C., et al. (2021). Electric field control of the magnetic Weyl fermion in an epitaxial $SrRuO_3$ (111) thin film. *Adv. Mater.* 33 (36), e2101316. doi:10.1002/adma.202101316

Liu, C., Yan, X., Jin, D., Ma, Y., Hsiao, H. W., Lin, Y., et al. (2021b). Two-dimensional superconductivity and anisotropic transport at $KTaO_3$ (111) interfaces. *Science* 371 (6530), 716–721. doi:10.1126/science.aba5511

Liu, J., Kriegner, D., Horak, L., Puggioni, D., Rayan Serrao, C., Chen, R., et al. (2016b). Strain-induced nonsymmorphic symmetry breaking and removal of Dirac semimetallic nodal line in an orthoperovskite iridate. *Phys. Rev. B* 93 (8), 085118. doi:10.1103/PhysRevB.93.085118

Liu, L., Qin, Q., Lin, W., Li, C., Xie, Q., He, S., et al. (2019). Current-induced magnetization switching in all-oxide heterostructures. *Nat. Nanotechnol.* 14 (10), 939–944. doi:10.1038/s41565-019-0534-7

Liu, L., Zhou, G., Shu, X., Li, C., Lin, W., Ren, L., et al. (2022). Room-temperature spin-orbit torque switching in a manganite-based heterostructure. *Phys. Rev. B.* 105 (14), 144419. doi:10.1103/PhysRevB.105.144419

Liu, Y.-T., Huang, C.-C., Chen, K.-H., Huang, Y. H., Tsai, C. C., Chang, T. Y., et al. (2021a). Anatomy of type-*x* spin-orbit-torque switching. *Phys. Rev. Appl.* 16 (2), 024021. doi:10.1103/PhysRevApplied.16.024021

Liu, Z. T., Li, M. Y., Li, Q. F., Liu, J. S., Li, W., Yang, H. F., et al. (2016a). Direct observation of the Dirac nodes lifting in semimetallic perovskite $SrIrO_3$ thin films. *Sci. Rep.* 6 (1), 30309. doi:10.1038/srep30309

Luke, G. M., Fudamoto, Y., Kojima, K. M., Larkin, M. I., Merrin, J., Nachumi, B., et al. (1998). Time-reversal symmetry-breaking superconductivity in Sr_2RuO_4. *Nature* 394 (6693), 558–561. doi:10.1038/29038

Ma, Q., Xu, S.-Y., Shen, H., MacNeill, D., Fatemi, V., Chang, T. R., et al. (2018). Observation of the nonlinear Hall effect under time-reversal-symmetric conditions. *Nature* 565 (7739), 337–342. doi:10.1038/s41586-018-0807-6

Manchon, A., Koo, H. C., Nitta, J., Frolov, S. M., and Duine, R. A. (2015). New perspectives for Rashba spin–orbit coupling. *Nat. Mater.* 14 (9), 871–882. doi:10.1038/nmat4360

Manchon, A., Železný, J., Miron, I. M., Jungwirth, T., Sinova, J., Thiaville, A., et al. (2019). Current-induced spin-orbit torques in ferromagnetic and antiferromagnetic systems. *Rev. Mod. Phys.* 91 (3), 035004. doi:10.1103/RevModPhys.91.035004

Manipatruni, S., Nikonov, D. E., and Young, I. A. (2018). Beyond CMOS computing with spin and polarization. *Nat. Phys.* 14 (4), 338–343. doi:10.1038/s41567-018-0101-4

Martínez, E. A., Dai, J., Tallarida, M., Nemes, N. M., and Bruno, F. Y (2023). Anisotropic electronic structure of the 2D electron gas at the $AlO_x/KTaO_3(110)$ interface. *Adv. Electron. Mater.* 9 (10), 2300267. doi:10.1002/aelm.202300267

Mathieu, R., Asamitsu, A., Yamada, H., Takahashi, K. S., Kawasaki, M., Fang, Z., et al. (2004). Scaling of the anomalous Hall effect in $Sr_{1-x}Ca_xRuO3$. *Phys. Rev. Lett.* 93 (1), 016602. doi:10.1103/PhysRevLett.93.016602

Mellnik, A. R., Lee, J. S., Richardella, A., Grab, J. L., Mintun, P. J., Fischer, M. H., et al. (2014). Spin-transfer torque generated by a topological insulator. *Nature* 511(7510): 449–451. doi:10.1038/nature13534

Moon, S. J., Jin, H., Kim, K. W., Choi, W. S., Lee, Y. S., Yu, J., et al. (2008). Dimensionality-controlled insulator-metal transition and correlated metallic state in 5*d* transition metal oxides $Sr_{n+1}Ir_nO_{3n+1}$(n=1, 2, and ∞). *Phys. Rev. Lett.* 101 (22), 226402. doi:10.1103/PhysRevLett.101.226402

Mosendz, O., Pearson, J. E., Fradin, F. Y., Bauer, G. E. W., Bader, S. D., and Hoffmann, A. (2010). Quantifying spin Hall angles from spin pumping: experiments and theory. *Phys. Rev. Lett.* 104 (4), 046601. doi:10.1103/PhysRevLett.104.046601

Nakamura, H., and Kimura, T. (2009). Electric field tuning of spin-orbit coupling in $KTaO_3$ field-effect transistors. *Phys. Rev. B* 80 (12), 121308. doi:10.1103/PhysRevB.80.121308

Nan, T., Anderson, T. J., Gibbons, J., Hwang, K., Campbell, N., Zhou, H., et al. (2019). Anisotropic spin-orbit torque generation in epitaxial $SrIrO_3$ by symmetry design. *Proc. Natl. Acad. Sci.* 116 (33), 16186–16191. doi:10.1073/pnas.1812822116

Nie, Y. F., King, P. D. C., Kim, C. H., Uchida, M., Wei, H., Faeth, B., et al. (2015). Interplay of spin-orbit interactions, dimensionality, and octahedral rotations in semimetallic $SrIrO_3$. *Phys. Rev. Lett.* 114 (1), 016401. doi:10.1103/PhysRevLett.114.016401

Noël, P., Trier, F., Vicente Arche, L. M., Bréhin, J., Vaz, D. C., Garcia, V., et al. (2020). Non-volatile electric control of spin–charge conversion in a $SrTiO_3$ Rashba system. *Nature* 580 (7804), 483–486. doi:10.1038/s41586-020-2197-9

Oh, Y.-W., Chris Baek, S.-h., Kim, Y. M., Lee, H. Y., Lee, K. D., Yang, C. G., et al. (2016). Field-free switching of perpendicular magnetization through spin–orbit torque in antiferromagnet/ferromagnet/oxide structures. *Nat. Nanotechnol.* 11 (10), 878–884. doi:10.1038/nnano.2016.109

Ohtomo, A., and Hwang, H. Y. (2004). A high-mobility electron gas at the $LaAlO_3/SrTiO_3$ heterointerface. *Nature* 427 (6973), 423–426. doi:10.1038/nature02308

Ou, Y., Wang, Z., Chang, C. S., Nair, H. P., Paik, H., Reynolds, N., et al. (2019). Exceptionally high, strongly temperature dependent, spin Hall conductivity of $SrRuO_3$. *Nano Lett.* 19 (6), 3663–3670. doi:10.1021/acs.nanolett.9b00729

Pai, Y.-Y., Tylan-Tyler, A., Irvin, P., and Levy, J. (2018). Physics of $SrTiO_3$-based heterostructures and nanostructures: a review. *Rep. Prog. Phys.* 81 (3), 036503. doi:10.1088/1361-6633/aa892d

Patri, A. S., Hwang, K., Lee, H.-W., and Kim, Y. B. (2018). Theory of large intrinsic spin Hall effect in iridate semimetals. *Sci. Rep.* 8 (1), 8052. doi:10.1038/s41598-018-26355-y

Ramesh, R., and Schlom, D. G. (2019). Creating emergent phenomena in oxide superlattices. *Nat. Rev. Mater.* 4 (4), 257–268. doi:10.1038/s41578-019-0095-2

Rao, W., Zhou, Y.-L., Wu, Y.-j., Duan, H. J., Deng, M. X., and Wang, R. Q. (2021). Theory for linear and nonlinear planar Hall effect in topological insulator thin films. *Phys. Rev. B* 103 (15), 155415. doi:10.1103/PhysRevB.103.155415

Ren, Z., Lao, B., Zheng, X., Liao, L., Lu, Z., Li, S., et al. (2022). Emergence of insulating ferrimagnetism and perpendicular magnetic anisotropy in 3*d*–5*d* perovskite oxide composite films for insulator spintronics. *ACS Appl. Mater. and Interfaces* 14 (13), 15407–15414. doi:10.1021/acsami.2c01849

Reyren, N., Thiel, S., Caviglia, A. D., Kourkoutis, L. F., Hammerl, G., Richter, C., et al. (2007). Superconducting interfaces between insulating oxides. *Science* 317 (5842), 1196–1199. doi:10.1126/science.1146006

Richter, T., Paleschke, M., Wahler, M., Heyroth, F., Deniz, H., Hesse, D., et al. (2017). Spin pumping and inverse spin Hall effect in ultrathin $SrRuO_3$ films around the percolation limit. *Phys. Rev. B* 96 (18), 184407. doi:10.1103/PhysRevB.96.184407

Santander-Syro, A. F., Bareille, C., Fortuna, F., Copie, O., Gabay, M., Bertran, F., et al. (2012). Orbital symmetry reconstruction and strong mass renormalization in the two-dimensional electron gas at the surface of $KTaO_3$. *Phys. Rev. B* 86 (12), 121107. doi:10.1103/PhysRevB.86.121107

Schilling, A., Cantoni, M., Guo, J. D., and Ott, H. R. (1993). Superconductivity above 130 K in the Hg–Ba–Ca–Cu–O system. *Nature* 363 (6424), 56–58. doi:10.1038/363056a0

Sinova, J., Culcer, D., Niu, Q., Sinitsyn, N. A., Jungwirth, T., and MacDonald, A. H. (2004). Universal intrinsic spin Hall effect. *Phys. Rev. Lett.* 92 (12), 126603. doi:10.1103/PhysRevLett.92.126603

Sinova, J., Valenzuela, S. O., Wunderlich, J., Back, C., and Jungwirth, T. (2015). Spin Hall effects. *Rev. Mod. Phys.* 87 (4), 1213–1260. doi:10.1103/RevModPhys.87.1213

Slonczewski, J. C. (1996). Current-driven excitation of magnetic multilayers. *J. Magnetism Magnetic Mater.* 159 (1), L1–L7. doi:10.1016/0304-8853(96)00062-5

Sodemann, I., and Fu, L. (2015). Quantum nonlinear Hall effect induced by Berry curvature dipole in time-reversal invariant materials. *Phys. Rev. Lett.* 115 (21), 216806. doi:10.1103/PhysRevLett.115.216806

Stemmer, S., and James Allen, S. (2014). Two-dimensional electron gases at complex oxide interfaces. *Annu. Rev. Mater. Res.* 44 (1), 151–171. doi:10.1146/annurev-matsci-070813-113552

Takiguchi, K., Wakabayashi, Y. K., Irie, H., Krockenberger, Y., Otsuka, T., Sawada, H., et al. (2020). Quantum transport evidence of Weyl fermions in an epitaxial ferromagnetic oxide. *Nat. Commun.* 11 (1), 4969. doi:10.1038/s41467-020-18646-8

Tang, A., Xu, T., Liu, S., Liang, Y., Chen, H., Yan, D., et al. (2022). Implementing complex oxides for efficient room-temperature spin–orbit torque switching. *Adv. Electron. Mater.* 8 (11), 2200514. doi:10.1002/aelm.202200514

Taniguchi, T., Mitani, S., and Hayashi, M. (2015). Critical current destabilizing perpendicular magnetization by the spin Hall effect. *Phys. Rev. B* 92 (2), 024428. doi:10.1103/PhysRevB.92.024428

Tian, D., Liu, Z., Shen, S., Li, Z., Zhou, Y., Liu, H., et al. (2021). Manipulating Berry curvature of $SrRuO_3$ thin films via epitaxial strain. *Proc. Natl. Acad. Sci.* 118 (18), e2101946118. doi:10.1073/pnas.2101946118

To, D. Q., Dang, T. H., Vila, L., Attané, J. P., Bibes, M., and Jaffrès, H. (2021). Spin to charge conversion at Rashba-split $SrTiO_3$ interfaces from resonant tunneling. *Phys. Rev. Res.* 3 (4), 043170. doi:10.1103/PhysRevResearch.3.043170

Tomioka, Y., Asamitsu, A., Moritomo, Y., and Tokura, Y. (1995). Anomalous magnetotransport properties of $Pr_{1-x}Ca_xMnO_3$. *J. Phys. Soc. Jpn.* 64 (10), 3626–3630. doi:10.1143/JPSJ.64.3626

Trier, F., Noël, P., Kim, J.-V., Attané, J. P., Vila, L., and Bibes, M. (2021). Oxide spin-orbitronics: spin–charge interconversion and topological spin textures. *Nat. Rev. Mater.* 7 (4), 258–274. doi:10.1038/s41578-021-00395-9

Trier, F., Prawiroatmodjo, G. E. D. K., Zhong, Z., Christensen, D. V., von Soosten, M., Bhowmik, A., et al. (2016). Quantization of Hall resistance at the metallic interface between an oxide insulator and $SrTiO_3$. *Phys. Rev. Lett.* 117 (9), 096804. doi:10.1103/PhysRevLett.117.096804

Trier, F., Vaz, D. C., Bruneel, P., Noël, P., Fert, A., Vila, L., et al. (2020). Electric-field control of spin current generation and detection in ferromagnet-free $SrTiO_3$-based nanodevices. *Nano Lett.* 20 (1), 395–401. doi:10.1021/acs.nanolett.9b04079

van Benthem, K., Elsässer, C., and French, R. H. (2001). Bulk electronic structure of $SrTiO_3$: experiment and theory. *J. Appl. Phys.* 90 (12), 6156–6164. doi:10.1063/1.1415766

Varotto, S., Johansson, A., Göbel, B., Vicente-Arche, L. M., Mallik, S., Bréhin, J., et al. (2022). Direct visualization of Rashba-split bands and spin/orbital-charge interconversion at $KTaO_3$ interfaces. *Nat. Commun.* 13 (1), 6165. doi:10.1038/s41467-022-33621-1

Vaz, D. C., Noël, P., Johansson, A., Göbel, B., Bruno, F. Y., Singh, G., et al. (2019). Mapping spin–charge conversion to the band structure in a topological oxide two-dimensional electron gas. *Nat. Mater.* 18 (11), 1187–1193. doi:10.1038/s41563-019-0467-4

Vicente-Arche, L. M., Bréhin, J., Varotto, S., Cosset-Cheneau, M., Mallik, S., Salazar, R., et al. (2021). Spin–charge interconversion in $KTaO_3$ 2D electron gases. *Adv. Mater.* 33 (43), e2102102. doi:10.1002/adma.202102102

Vrejoiu, I., Le Rhun, G., Pintilie, L., Hesse, D., Alexe, M., and Gösele, U. (2006). Intrinsic ferroelectric properties of strained tetragonal $PbZr_{0.2}Ti_{0.8}O_3$ obtained on layer–by–layer grown, defect–free single–crystalline films. *Adv. Mater.* 18 (13), 1657–1661. doi:10.1002/adma.200502711

Wadehra, N., Tomar, R., Varma, R. M., Gopal, R. K., Singh, Y., Dattagupta, S., et al. (2020). Planar Hall effect and anisotropic magnetoresistance in polar-polar interface of $LaVO_3$-$KTaO_3$ with strong spin-orbit coupling. *Nat. Commun.* 11 (1), 874. doi:10.1038/s41467-020-14689-z

Wahler, M., Homonnay, N., Richter, T., Müller, A., Eisenschmidt, C., Fuhrmann, B., et al. (2016). Inverse spin Hall effect in a complex ferromagnetic oxide heterostructure. *Sci. Rep.* 6 (1), 28727. doi:10.1038/srep28727

Wang, H., Meng, K.-Y., Zhang, P., Hou, J. T., Finley, J., Han, J., et al. (2019). Large spin-orbit torque observed in epitaxial $SrIrO_3$ thin films. *Appl. Phys. Lett.* 114 (23). doi:10.1063/1.5097699

Wang, Y., Ramaswamy, R., Motapothula, M., Narayanapillai, K., Zhu, D., Yu, J., et al. (2017). Room-temperature giant charge-to-spin conversion at the $SrTiO_3$–$LaAlO_3$ oxide interface. *Nano Lett.* 17 (12), 7659–7664. doi:10.1021/acs.nanolett.7b03714

Wang, Z., Zhong, Z., Hao, X., Gerhold, S., Stöger, B., Schmid, M., et al. (2014). Anisotropic two-dimensional electron gas at $SrTiO_3$(110). *Proc. Natl. Acad. Sci.* 111 (11), 3933–3937. doi:10.1073/pnas.1318304111

Wei, J., Zhong, H., Liu, J., Wang, X., Meng, F., Xu, H., et al. (2021). Enhancement of spin–orbit torque by strain engineering in $SrRuO_3$ films. *Adv. Funct. Mater.* 31 (40). doi:10.1002/adfm.202100380

Witczak-Krempa, W., Chen, G., Kim, Y. B., and Balents, L. (2014). Correlated quantum phenomena in the strong spin-orbit regime. *Annu. Rev. Condens. Matter Phys.* 5 (1), 57–82. doi:10.1146/annurev-conmatphys-020911-125138

Xiao, D., Chang, M.-C., and Niu, Q. (2010). Berry phase effects on electronic properties. *Rev. Mod. Phys.* 82 (3), 1959–2007. doi:10.1103/RevModPhys.82.1959

Yan, B., and Felser, C. (2017). Topological materials: Weyl semimetals. *Annu. Rev. Condens. Matter Phys.* 8 (1), 337–354. doi:10.1146/annurev-conmatphys-031016-025458

Yasuda, K., Tsukazaki, A., Yoshimi, R., Kondou, K., Takahashi, K., Otani, Y., et al. (2017). Current-nonlinear Hall effect and spin-orbit torque magnetization switching in a magnetic topological insulator. *Phys. Rev. Lett.* 119 (13), 137204. doi:10.1103/PhysRevLett.119.137204

Yoon, J., Lee, S.-W., Kwon, J. H., Lee, J. M., Son, J., Qiu, X., et al. (2017). Anomalous spin-orbit torque switching due to field-like torque–assisted domain wall reflection. *Sci. Adv.* 3 (4), e1603099. doi:10.1126/sciadv.1603099

Yu, G., Upadhyaya, P., Fan, Y., Alzate, J. G., Jiang, W., Wong, K. L., et al. (2014). Switching of perpendicular magnetization by spin–orbit torques in the absence of external magnetic fields. *Nat. Nanotechnol.* 9 (7), 548–554. doi:10.1038/nnano.2014.94

Yu, X.-Q., Zhu, Z.-G., and Su, G. (2021). Hexagonal warping induced nonlinear planar Nernst effect in nonmagnetic topological insulators. *Phys. Rev. B* 103 (3), 035410. doi:10.1103/PhysRevB.103.035410

Zhang, H., Ma, Y., Zhang, H., Chen, X., Wang, S., Li, G., et al. (2019b). Thermal spin injection and inverse Edelstein effect of the two-dimensional electron gas at EuO–$KTaO_3$ interfaces. *Nano Lett.* 19 (3), 1605–1612. doi:10.1021/acs.nanolett.8b04509

Zhang, H., Yan, X., Zhang, X., Wang, S., Xiong, C., Zhang, H., et al. (2019a). Unusual electric and optical tuning of $KTaO_3$-based two-dimensional electron gases with 5*d* orbitals. *ACS Nano* 13 (1), 609–615. doi:10.1021/acsnano.8b07622

Zhang, H., Yun, Y., Zhang, X., Zhang, H., Ma, Y., Yan, X., et al. (2018). High-mobility spin-polarized two-dimensional electron gases at EuO/$KTaO_3$ interfaces. *Phys. Rev. Lett.* 121 (11), 116803. doi:10.1103/PhysRevLett.121.116803

Zhang, H., Zhang, H., Yan, X., Zhang, X., Zhang, Q., Zhang, J., et al. (2017). Highly mobile two-dimensional electron gases with a strong gating effect at the amorphous $LaAlO_3$/$KTaO_3$ interface. *ACS Appl. Mater. and Interfaces* 9 (41), 36456–36461. doi:10.1021/acsami.7b12814

Zhang, H., Zhu, Z., Zhu, Y., Chen, X., Jiang, Q., Wei, J., et al. (2023). Fermi-level-dependent charge-to-spin conversion of the two-dimensional electron gas at the γ-Al_2O_3/$KTaO_3$ interface. *Phys. Rev. Appl.* 19 (3), 034045. doi:10.1103/PhysRevApplied.19.034045

Zhang, J., Zhang, J., Chi, X., Hao, R., Chen, W., Yang, H., et al. (2022). Giant efficiency for charge-to-spin conversion via the electron gas at the $LaTiO_{3+\delta}$/$SrTiO_3$ interface. *Phys. Rev. B* 105 (19), 195110. doi:10.1103/PhysRevB.105.195110

Zhang, Q., Shi, S., Zheng, Z., Zhou, H., Shao, D. F., Zhao, T., et al. (2024a). Highly energy-efficient spin current generation in $SrIrO_3$ by manipulating the octahedral rotation. *ACS Appl. Mater. and Interfaces* 16 (1), 1129–1136. doi:10.1021/acsami.3c15514

Zhang, S., Levy, P. M., and Fert, A. (2002). Mechanisms of spin-polarized current-driven magnetization switching. *Phys. Rev. Lett.* 88 (23), 236601. doi:10.1103/PhysRevLett.88.236601

Zhang, X., Zhu, T., Zhang, S., Chen, Z., Song, A., Zhang, C., et al. (2024b). Light-induced giant enhancement of nonreciprocal transport at $KTaO_3$-based interfaces. *Nat. Commun.* 15 (1), 2992. doi:10.1038/s41467-024-47231-6

Zhao, K., Li, S., Lu, Z., Lao, B., Zheng, X., Li, R. W., et al. (2024). Crystal orientation regulation of spin-orbit torque efficiency and magnetization switching in $SrRuO_3$ thin films. *Acta Phys. Sin.* 0 (0), 117701. doi:10.7498/aps.73.20240367

Zheng, Z., Zhang, Y., Lopez-Dominguez, V., Sánchez-Tejerina, L., Shi, J., Feng, X., et al. (2021). Field-free spin-orbit torque-induced switching of perpendicular magnetization in a ferrimagnetic layer with a vertical composition gradient. *Nat. Commun.* 12 (1), 4555. doi:10.1038/s41467-021-24854-7

Zhou, J., Shu, X., Lin, W., Shao, D. F., Chen, S., Liu, L., et al. (2021). Modulation of spin–orbit torque from $SrRuO_3$ by epitaxial-strain-induced octahedral rotation. *Adv. Mater.* 33 (30), e2007114. doi:10.1002/adma.202007114

Zhu, D., and Zhao, W. (2020). Threshold current density for perpendicular magnetization switching through spin-orbit torque. *Phys. Rev. Appl.* 13 (4), 044078. doi:10.1103/PhysRevApplied.13.044078

Zou, K., Ismail-Beigi, S., Kisslinger, K., Shen, X., Su, D., Walker, F. J., et al. (2015). $LaTiO_3$/$KTaO_3$ interfaces: a new two-dimensional electron gas system. *Apl. Mater.* 3 (3). doi:10.1063/1.4914310